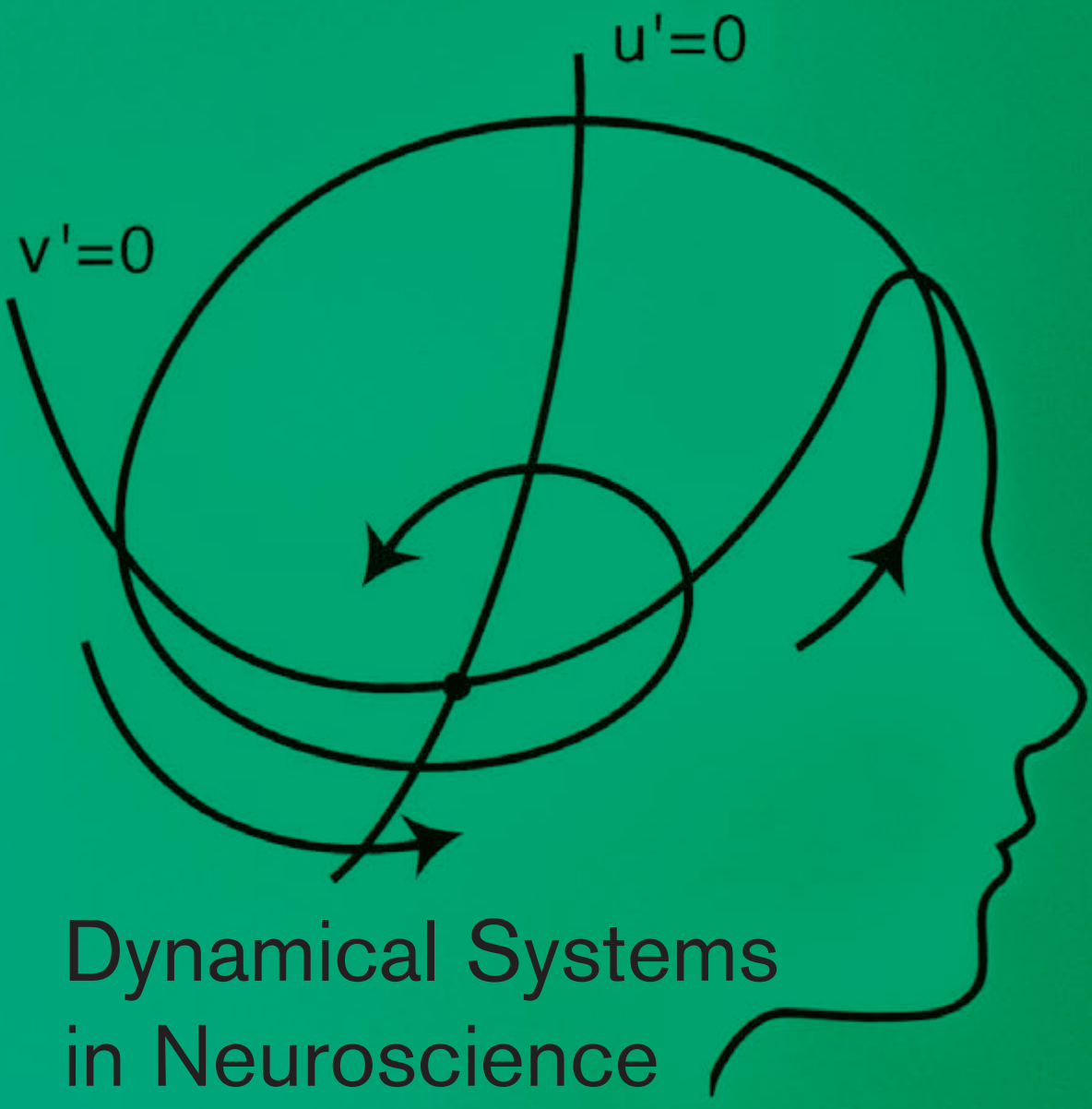

Dynamical Systems in Neuroscience

The Geometry of Excitability and Bursting

Eugene M. Izhikevich

Dynamical Systems in Neuroscience

Computational Neuroscience

Terrence J. Sejnowski and Tomaso A. Poggio, editors

Neural Nets in Electric Fish, Walter Heiligenberg, 1991

The Computational Brain, Patricia S. Churchland and Terrence J. Sejnowski, 1992

Dynamic Biological Networks: The Stomatogastric Nervous System, edited by Ronald M. Harris-Warrick, Eve Marder, Allen I. Selverston, and Maurice Maulins, 1992

The Neurobiology of Neural Networks, edited by Daniel Gardner, 1993

Large-Scale Neuronal Theories of the Brain, edited by Christof Koch and Joel L. Davis, 1994

The Theoretical Foundations of Dendritic Function: Selected Papers of Wilfrid Rall with Commentaries, edited by Idan Segev, John Rinzel, and Gordon M. Shepherd, 1995

Models of Information Processing in the Basal Ganglia, edited by James C. Houk, Joel L. Davis, and David G. Beiser, 1995

Spikes: Exploring the Neural Code, Fred Rieke, David Warland, Rob de Ruyter van Stevenick, and William Bialek, 1997

Neurons, Networks, and Motor Behavior, edited by Paul S. Stein, Sten Grillner, Allen I. Selverston, and Douglas G. Stuart, 1997

Methods in Neuronal Modeling: From Ions to Networks, second edition, edited by Christof Koch and Idan Segev, 1998

Fundamentals of Neural Network Modeling: Neuropsychology and Cognitive Neuroscience, edited by Randolph W. Parks, Daniel S. Levin, and Debra L. Long, 1998

Neural Codes and Distributed Representations: Foundations of Neural Computation, edited by Laurence Abbott and Terrence J. Sejnowski, 1999

Unsupervised Learning: Foundations of Neural Computation, edited by Geoffrey Hinton and Terrence J. Sejnowski, 1999

Fast Oscillations in Cortical Circuits, Roger D. Traub, John G.R. Jefferys, and Miles Al Whittington, 1999

Computational Vision: Information Processing in Perception and Visual Behavior, Hanspeter A. Mallot, 2000

Graphical Models: Foundations of Neural Computation, edited by Michael I. Jordan and Terrence J. Sejnowski, 2001

Self-Organizing Map Formation: Foundation of Neural Computation, edited by Klaus Obermayer and Terrence J. Sejnowski, 2001

Theoretical Neuroscience: Computational and Mathematical Modeling of Neural Systems, Peter Dayan and L. F. Abbott, 2001

Neural Engineering: Computation, Representation, and Dynamics in Neurobiological Systems, Chris Eliasmith and Charles H. Anderson, 2003

The Computational Neurobiology of Reaching and Pointing, edited by Reza Shadmehr and Steven P. Wise, 2005

Dynamical Systems in Neuroscience: The Geometry of Excitability and Bursting, Eugene M. Izhikevich, 2007

Dynamical Systems in Neuroscience:
The Geometry of Excitability and Bursting

Eugene M. Izhikevich

The MIT Press
Cambridge, Massachusetts
London, England

This book was set in LaTeX by the author. Printed and bound in the United States of America.

Library of Congress Cataloging-in-Publication Data

Izhikevich, Eugene M., 1967–
Dynamical systems in neuroscience: the geometry of excitability and bursting / Eugene M. Izhikevich.
p. cm. — (Computational neuroscience)
Includes bibliographical references and index.
ISBN 978-0-262-09043-8 (hc. : alk. paper)
1. Neural networks (Neurobiology) 2. Neurons - computer simulation. 3. Dynamical systems. 4. Computational neuroscience. I. Izhikevich, E. M. II Title. III. Series.

QP363.3.I94 2007
573.8'01'13—DC21 2006040349

10 9 8 7 6 5 4 3 2 1

To my beautiful daughters, Liz and Kate.

Contents

Preface

Historically, much of theoretical neuroscience research concerned neuronal circuits and synaptic organization. The neurons were divided into excitatory and inhibitory types, but their electrophysiological properties were largely neglected or taken to be identical to those of Hodgkin-Huxley's squid axon. The present awareness of the importance of the electrophysiology of individual neurons is best summarized by David McCormick in the fifth edition of Gordon Shepherd's book *The Synaptic Organization of the Brain*:

> Information-processing depends not only on the *anatomical* substrates of synaptic circuits but also on the *electrophysiological* properties of neurons... Even if two neurons in different regions of the nervous system possess identical morphological features, they may respond to the same synaptic input in very different manners because of each cell's intrinsic properties.
>
> McCormick (2004)

Much of present neuroscience research concerns voltage- and second-messenger-gated currents in individual cells, with the goal of understanding the cell's intrinsic neurocomputational properties. It is widely accepted that knowing the currents suffices to determine what the cell is doing and why it is doing it. This, however, contradicts a half-century–old observation that cells having similar currents can nevertheless exhibit quite different dynamics. Indeed, studying isolated axons having presumably similar electrophysiology (all are from the crustacean *Carcinus maenas*), Hodgkin (1948) injected a DC-current of varying amplitude, and discovered that some preparations could exhibit repetitive spiking with arbitrarily low frequencies, while the others discharged in a narrow frequency band. This observation was largely ignored by the neuroscience community until the seminal paper by Rinzel and Ermentrout (1989), who showed that the difference in behavior is due to different *bifurcation* mechanisms of excitability.

Let us treat the amplitude of the injected current in Hodgkin's experiments as a bifurcation parameter: When the amplitude is small, the cell is quiescent; when the amplitude is large, the cell fires repetitive spikes. When we change the amplitude of the injected current, the cell undergoes a transition from quiescence to repetitive spiking. From the dynamical systems point of view, the transition corresponds to a bifurcation from equilibrium to a limit cycle attractor. The type of bifurcation determines the most fundamental computational properties of neurons, such as the class of excitability, the existence or nonexistence of threshold, all-or-none spikes, subthreshold oscillations, the ability to generate postinhibitory rebound spikes, bistability of resting and spiking states, whether the neuron is an integrator or a resonator, and so on.

This book is devoted to a systematic study of the relationship between electrophysiology, bifurcations, and computational properties of neurons. The reader will learn why cells having nearly identical currents may undergo distinct bifurcations, and hence they will have fundamentally different neurocomputational properties. (Conversely, cells

having quite different currents may undergo identical bifurcations, and hence they will have similar neurocomputational properties.) The major message of the book can be summarized as follows (compare with the McCormick statement above):

> Information-processing depends not only on the electrophysiological properties of neurons but also on their *dynamical properties*. Even if two neurons in the same region of the nervous system possess similar electrophysiological features, they may respond to the same synaptic input in very different manners because of each cell's bifurcation dynamics.

Nonlinear dynamical system theory is a core of computational neuroscience research, but it is not a standard part of the graduate neuroscience curriculum. Neither is it taught in most math/physics departments in a form suitable for a general biological audience. As a result, many neuroscientists fail to grasp such fundamental concepts as equilibrium, stability, limit cycle attractor, and bifurcations, even though neuroscientists constantly encounter these nonlinear phenomena.

This book introduces dynamical systems starting with simple one- and two-dimensional spiking models and continuing all the way to bursting systems. Each chapter is organized from simple to complex, so everybody can start reading the book; only the reader's background will determine where he or she stops. The book emphasizes the geometrical approach, so there are few equations but a lot of figures. Half of them are simulations of various neural models, so there are hundreds of possible exercises such as "Use MATLAB (GENESIS, NEURON, XPPAUT, etc.) and parameters in the caption of figure X to simulate the figure." Additional problems are provided at the end of each chapter; the reader is encouraged to solve at least some of them and to look at the solutions of the others at the end of the book. Problems marked [**M.S.**] or [**Ph.D.**] are suggested thesis topics.

Acknowledgments. I thank the scientists who reviewed the first draft of the book: Pablo Achard, Jose M. Amigo, Vlatko Becanovic, Brent Doiron, George Bard Ermentrout, Richard FitzHugh, David Golomb, Andrei Iacob, Paul Kulchenko, Maciej Lazarewicz, Georgi Medvedev, John Rinzel, Anil K. Seth, Gautam C Sethia, Arthur Sherman, Klaus M. Stiefel, and Takashi Tateno. I also thank the anonymous referees who peer-reviewed the book and made quite a few valuable suggestions instead of just rejecting it. Special thanks go to Niraj S. Desai, who made most of the in vitro recordings used in the book (the data are available on the author's Web page `www.izhikevich.com`), and to Bruno van Swinderen, who drew the cartoons. I enjoyed the hospitality of The Neurosciences Institute – a monastery of interdisciplinary science – and I benefited greatly from the expertise and support of its fellows.

Finally, I thank my wife, Tatyana, and my wonderful daughters, Elizabeth and Kate, for their support and patience during the five-year gestation of this book.

Eugene M. Izhikevich
San Diego, California

`www.izhikevich.com`
December 19, 2005

Chapter 1

Introduction

This chapter highlights some of the most important concepts developed in the book. First, we discuss several common misconceptions regarding the spike generation mechanism of neurons. Our goal is to motivate the reader to think of a neuron not only in terms of ions and channels, as many biologists do, and not only in terms of an input/output relationship, as many theoreticians do, but also as a nonlinear dynamical system that looks at the input through the prism of its own intrinsic dynamics. We ask such questions as "What makes a neuron fire?" or "Where is the threshold?", and then outline the answers, using the geometrical theory of dynamical systems.

From a dynamical systems point of view, neurons are excitable because they are near a transition, called bifurcation, from resting to sustained spiking activity. While there is a huge number of possible ionic mechanisms of excitability and spike generation, there are only four bifurcation mechanisms that can result in such a transition. Considering the geometry of phase portraits at these bifurcations, we can understand many computational properties of neurons, such as the nature of threshold and all-or-none spiking, the coexistence of resting and spiking states, the origin of spike latencies, postinhibitory spikes, and the mechanism of integration and resonance. Moreover, we can understand how these properties are interrelated, why some are equivalent, and why some are mutually exclusive.

1.1 Neurons

If somebody were to put a gun to the head of the author of this book and ask him to name the single most important concept in brain science, he would say it is the concept of a *neuron*. There are only 10^{11} or so neurons in the human brain, much fewer than the number of non-neural cells such as glia. Yet neurons are unique in the sense that only they can transmit electrical signals over long distances. From the neuronal level we can go down to cell biophysics and to the molecular biology of gene regulation. From the neuronal level we can go up to neuronal circuits, to cortical structures, to the whole brain, and finally to the behavior of the organism. So let us see how much we understand of what is going on at the level of individual neurons.

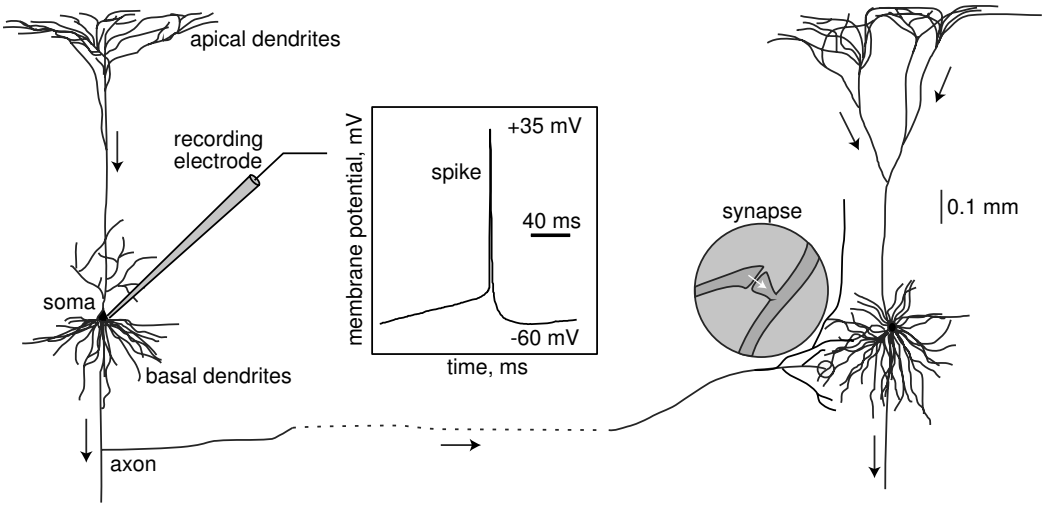

Figure 1.1: Two interconnected cortical pyramidal neurons (hand drawing) and in vitro recorded spike.

1.1.1 What Is a Spike?

A typical neuron receives inputs from more than $10,000$ other neurons through the contacts on its dendritic tree called synapses; see Fig.1.1. The inputs produce electrical transmembrane currents that change the membrane potential of the neuron. Synaptic currents produce changes, called postsynaptic potentials (PSPs). Small currents produce small PSPs; larger currents produce significant PSPs that can be amplified by the voltage-sensitive channels embedded in the neuronal membrane and lead to the generation of an *action potential* or *spike* – an abrupt and transient change of membrane voltage that propagates to other neurons via a long protrusion called an axon.

Such spikes are the main means of communication between neurons. In general, neurons do not fire on their own; they fire as a result of incoming spikes from other neurons. One of the most fundamental questions of neuroscience is *What, exactly, makes neurons fire?* What is it in the incoming pulses that elicits a response in one neuron but not in another? Why can two neurons have different responses to exactly the same input and identical responses to completely different inputs? To answer these questions, we need to understand the dynamics of spike generation mechanisms of neurons.

Most introductory neuroscience books describe neurons as integrators with a threshold: neurons sum incoming PSPs and "compare" the integrated PSP with a certain voltage value, called the firing threshold. If it is below the threshold, the neuron remains quiescent; when it is above the threshold, the neuron fires an all-or-none spike, as in Fig.1.3, and resets its membrane potential. To add theoretical plausibility to this argument, the books refer to the Hodgkin-Huxley model of spike generation in squid

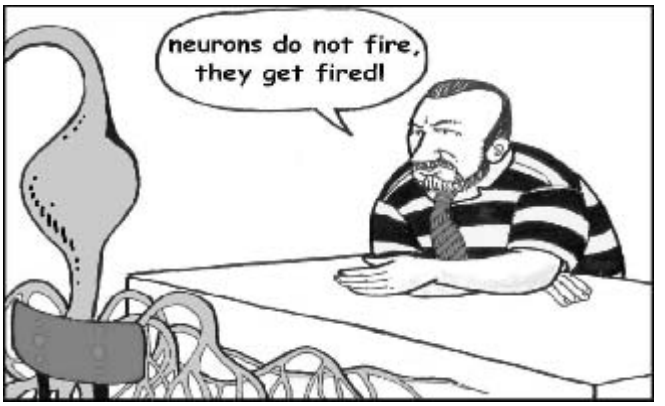

Figure 1.2: What makes a neuron fire?

giant axons, which we study in chapter 2. The irony is that the Hodgkin-Huxley model does not have a well-defined threshold; it does not fire all-or-none spikes; and it is not an integrator, but a resonator (i.e., it prefers inputs having certain frequencies that resonate with the frequency of subthreshold oscillations of the neuron). We consider these and other properties in detail in this book.

1.1.2 Where Is the Threshold?

Much effort has been spent trying to experimentally determine the firing thresholds of neurons. Here, we challenge the classical view of a threshold. Let us consider two typical experiments, depicted in Fig.1.4, that are designed to measure the threshold. in Fig.1.4a, we shock a cortical neuron (i.e., we inject brief but strong pulses of current of various amplitudes to depolarize the membrane potential to various values). Is there a clear-cut voltage value, as in Fig.1.3, above which the neuron fires but below which no spikes occur? If you find one, let the author know! In Fig.1.4b we inject long but weak pulses of current of various amplitudes, which results in slow depolarization and a spike. The firing threshold, if it exists, must be somewhere in the shaded region, but where? Where does the slow depolarization end and the spike start? Is it meaningful to talk about firing thresholds at all?

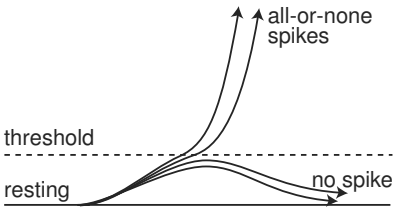

Figure 1.3: The concept of a firing threshold.

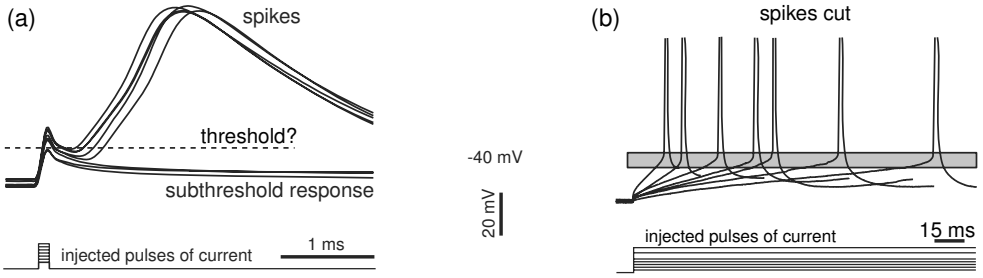

Figure 1.4: Where is the firing threshold? Shown are in vitro recordings of two layer 5 rat pyramidal neurons. Notice the differences of voltage and time scales.

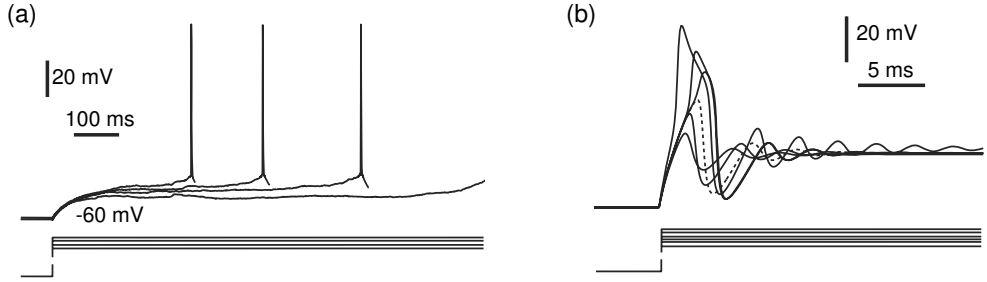

Figure 1.5: Where is the rheobase (i.e., the minimal current that fires the cell)? (a) in vitro recordings of the pyramidal neuron of layer 2/3 of a rat's visual cortex show increasing latencies as the amplitude of the injected current decreases. (b) Simulation of the $I_{\mathrm{Na,p}}$+I_{K}−model (pronounced: *persistent sodium plus potassium model*) shows spikes of graded amplitude.

Perhaps, we should measure current thresholds instead of voltage thresholds. The current threshold (i.e., the minimal amplitude of injected current of infinite duration needed to fire a neuron) is called the *rheobase*. In Fig.1.5 we decrease the amplitudes of injected pulses of current to find the minimal one that still elicits a spike or the maximal one that does not. In Fig.1.5a, progressively weaker pulses result in longer latencies to the first spike. Eventually the neuron does not fire because the latency is longer than the duration of the pulse, which is 1 second in the figure. Did we really measure the neuronal rheobase? What if we waited a bit longer? How long is long enough? In Fig.1.5b the latencies do not grow, but the spike amplitudes decrease until the spikes do not look like spikes at all. To determine the current threshold, we need to draw the line and separate spike responses from "subthreshold" ones. How can we do that if the spikes are not all-or-none? Is the response denoted by the dashed line a spike?

Risking adding more confusion to the notion of a threshold, consider the following. If excitatory inputs depolarize the membrane potential (i.e., bring it closer to

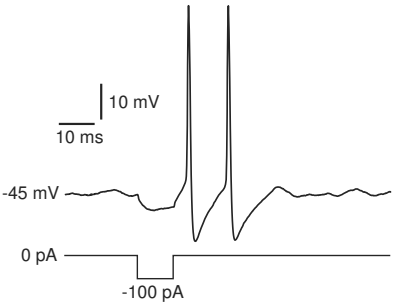

Figure 1.6: In vitro recording of rebound spikes of a rat's brainstem mesV neuron in response to a brief hyperpolarizing pulse of current.

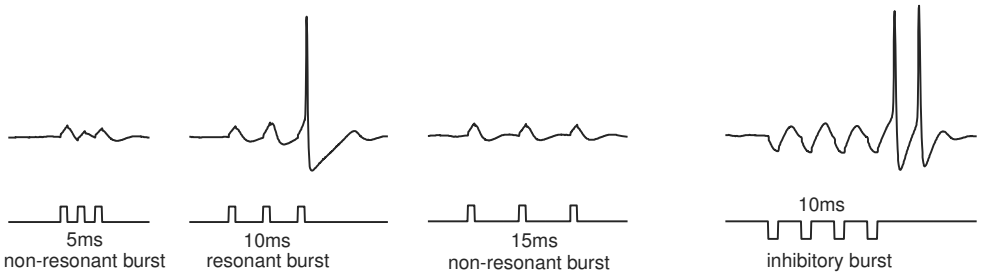

Figure 1.7: Resonant response of the mesencephalic V neuron of a rat's brainstem to pulses of injected current having a 10 ms period (in vitro).

the "firing threshold"), and inhibitory inputs hyperpolarize the potential and move it away from the threshold, then *how can the neuron in Fig.1.6 fire in response to the inhibitory input?* This phenomenon, also observed in the Hodgkin-Huxley model, is called anodal break excitation, rebound spike, or postinhibitory spike. Many biologists say that rebound responses are due to the activation and inactivation of certain slow currents, which bring the membrane potential over the threshold or, equivalently, lower the threshold upon release from the hyperpolarization – a phenomenon called a low-threshold spike in thalamocortical neurons. The problem with this explanation is that neither the Hodgkin-Huxley model nor the neuron in Fig.1.6 has these currents, and even if they did, the hyperpolarization is too short and too weak to affect the currents.

Another interesting phenomenon is depicted in Fig.1.7. The neuron is stimulated with brief pulses of current mimicking an incoming burst of three spikes. When the stimulation frequency is high (5 ms period), presumably reflecting a strong input, the neuron does not fire at all. However, stimulation with a lower frequency (10 ms period) that resonates with the frequency of subthreshold oscillation of the neuron evokes a spike response, regardless of whether the stimulation is excitatory or inhibitory. Stimulation with even lower frequency (15 ms period) cannot elicit spike response again. Thus, the neuron is sensitive only to the inputs having resonant frequency. The same pulses applied to a cortical pyramidal neuron evoke a response only in the first case (small period), but not in the other cases.

1.1.3 Why Are Neurons Different, and Why Do We Care?

Why would two neurons respond completely differently to the same input? A biologist would say that the response of a neuron depends on many factors, such as the type of voltage- and Ca^{2+}-gated channels expressed by the neuron, the morphology of its dendritic tree, the location of the input, and other factors. These factors are indeed important, but they do not determine the neuronal response per se. Rather they determine the rules that govern dynamics of the neuron. Different conductances and currents can result in the same rules, and hence in the same responses; conversely, similar currents can result in different rules and in different responses. The currents define what kind of dynamical system the neuron is.

We study ionic transmembrane currents in chapter 2. In subsequent chapters we investigate how the types of currents determine neuronal dynamics. We divide all currents into two major classes: amplifying and resonant, with the persistent Na^+ current $I_{Na,p}$ and the persistent K^+ current I_K being the typical examples of the former and the latter, respectively. Since there are tens of known currents, purely combinatorial argument implies that there are millions of different electrophysiological mechanisms of spike generation. We will show later that any such mechanism must have at least one amplifying and one resonant current. Some mechanisms, called minimal in this book, have one resonant and one amplifying current. They provide an invaluable tool in classifying and understanding the electrophysiology of spike generation.

Many illustrations in this book are based on simulations of the reduced $I_{Na,p} + I_K$-model (pronounced *persistent sodium plus potassium model*), which consists of a fast persistent Na^+ (amplifying) current and a slower persistent K^+ (resonant) current. It is equivalent to the famous and widely used Morris-Lecar $I_{Ca}+I_K$-model (Morris and Lecar 1981). We show that the model exhibits quite different dynamics, depending on the values of the parameters, e.g., the half-activation voltage of the K^+ current: in one case, it can fire in a narrow frequency range, it can exhibit coexistence of resting and spiking states, and it has damped subthreshold oscillations of membrane potential. In another case, it can fire in a wide frequency range and show no coexistence of resting and spiking and no subthreshold oscillations. Thus, seemingly inessential differences in parameter values could result in drastically distinct behaviors.

1.1.4 Building Models

To build a good model of a neuron, electrophysiologists apply different pharmacological blockers to tease out the currents that the neuron has. Then they apply different stimulation protocols to measure the kinetic parameters of the currents, such as the Boltzmann activation function, time constants, and maximal conductances. We consider all these functions in chapter 2. Next, they create a Hodgkin-Huxley-type model and simulate it using the NEURON, GENESIS, or XPP environment or MATLAB (the first two are invaluable tools for simulating realistic dendritic structures).

The problem is that the parameters are measured in different neurons and then put together into a single model. As an illustration, consider two neurons having the same

Figure 1.8: Neurons are dynamical systems.

currents, say $I_{\mathrm{Na,p}}$ and I_{K}, and exhibiting excitable behavior; that is, both neurons are quiescent but can fire a spike in response to a stimulation. Suppose the second neuron has stronger $I_{\mathrm{Na,p}}$, which is balanced by stronger I_{K}. If we measure Na^+ conductance using the first neuron and K^+ conductance using the second neuron, the resulting $I_{\mathrm{Na,p}} + I_{\mathrm{K}}$-model will have an excess of K^+ current and probably will not be able to fire spikes at all. Conversely, if we measure Na^+ and K^+ conductances using the second neuron and then the first neuron, respectively, the model would have too much Na^+ current and probably would exhibit sustained pacemaking activity. In any case, the model fails to reproduce the excitable behavior of the neurons whose parameters we measured.

Some of the parameters cannot be measured at all, so many arbitrary choices are made via a process called "fine-tuning". Navigating in the dark, possibly with the help of some biological intuition, the researcher modifies parameters, compares simulations with experiment, and repeats this trial-and-error procedure until he or she is satisfied with the results. Since seemingly similar values of parameters can result in drastically different behaviors, and quite different parameters can result in seemingly similar behaviors, how do we know that the resulting model is correct? How do we know that its behavior is equivalent to that of the neuron we want to study? And what is *equivalent* in this case? Now, you are primed to consider dynamical systems. If not, see Fig.1.8.

1.2 Dynamical Systems

In chapter 2 we introduce the Hodgkin-Huxley formalism to describe neuronal dynamics in terms of activation and inactivation of voltage-gated conductances. An important result of the Hodgkin-Huxley studies is that *neurons are dynamical systems*, so they should be studied as such. Below we mention some of the important concepts of dynamical systems theory. The reader does not have to follow all the details of this section because the concepts are explained in greater detail in subsequent chapters.

A dynamical system consists of a set of variables that describe its state and a law that describes the evolution of the state variables with time (i.e., how the state of the system in the next moment of time depends on the input and its state in the previous moment of time). The Hodgkin-Huxley model is a four-dimensional dynamical system because its state is uniquely determined by the membrane potential, V, and so-called gating variables n, m, and h for persistent K^+ and transient Na^+ currents. The evolution law is given by a four-dimensional system of ordinary differential equations.

Typically, all variables describing neuronal dynamics can be classified into four classes, according to their function and the time scale.

1. *Membrane potential.*

2. *Excitation variables*, such as activation of a Na^+ current. These variables are responsible for the upstroke of the spike.

3. *Recovery variables*, such as inactivation of a Na^+ current and activation of a fast K^+ current. These variables are responsible for the repolarization (downstroke) of the spike.

4. *Adaptation variables*, such as activation of slow voltage- or Ca^{2+}-dependent currents. These variables build up during prolonged spiking and can affect excitability in the long run.

The Hodgkin-Huxley model does not have variables of the fourth type, but many neuronal models do, especially those exhibiting bursting dynamics.

1.2.1 Phase Portraits

The power of the dynamical systems approach to neuroscience, as well as to many other sciences, is that we can tell something, or many things, about a system without knowing all the details that govern the system evolution. We do not even use equations to do that! Some may even wonder why we call it a mathematical theory.

As a start, let us consider a quiescent neuron whose membrane potential is resting. From the dynamical systems point of view, there are no changes of the state variables of such a neuron; hence it is at an equilibrium point. All the inward currents that depolarize the neuron are balanced, or equilibrated, by the outward currents that hyperpolarize it. If the neuron remains quiescent despite small disturbances and membrane noise, as in Fig.1.9a (top), then we conclude that the equilibrium is stable. Isn't

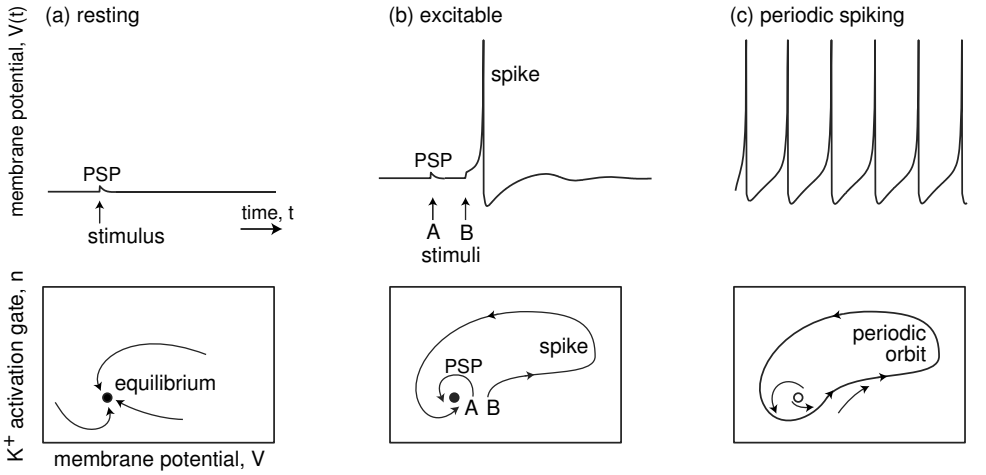

Figure 1.9: Resting, excitable, and periodic spiking activity correspond to a stable equilibrium (a and b) or limit cycle (c), respectively.

it amazing that we can reach such a conclusion without knowing the equations that describe the neuron's dynamics? We do not even know the number of variables needed to describe the neuron; it could be infinite, for all we care.

In this book we introduce the notions of equilibria, stability, threshold, and attraction domains using one- and two-dimensional dynamical systems, e.g., the $I_{\mathrm{Na,p}}$+I_{K}-model with instantaneous Na^+ kinetics. The state of this model is described by the membrane potential, V, and the activation variable, n, of the persistent K^+ current, so it is a two-dimensional vector (V, n). Instantaneous activation of the Na^+ current is a function of V, so it does not result in a separate variable of the model. The evolution of the model is a trajectory $(V(t), n(t))$ on the $V \times n-$plane. Depending on the initial point, the system can have many trajectories, such as those depicted in Fig.1.9a (bottom). Time is not explicitly present in the figure, but units of time may be thought of as plotted along each trajectory. All of the trajectories in the figure are attracted to the stable equilibrium denoted by the black dot, called an *attractor*. The overall qualitative description of dynamics can be obtained through the study of the *phase portrait* of the system, which depicts certain special trajectories (equilibria, separatrices, limit cycles) that determine the topological behavior of all the other trajectories in the phase space. Probably 50 percent of illustrations in this book are phase portraits.

A fundamental property of neurons is *excitability*, illustrated in Fig.1.9b. The neuron is resting, i.e., its phase portrait has a stable equilibrium. Small perturbations, such as A, result in small excursions from the equilibrium, denoted as PSP (postsynaptic potential). Larger perturbations, such as B, are amplified by the neuron's intrinsic dynamics and result in the spike response. To understand the dynamic mechanism of such amplification, we need to consider the geometry of the phase portrait near the resting equilibrium, i.e., in the region where the decision to fire or not to fire is made.

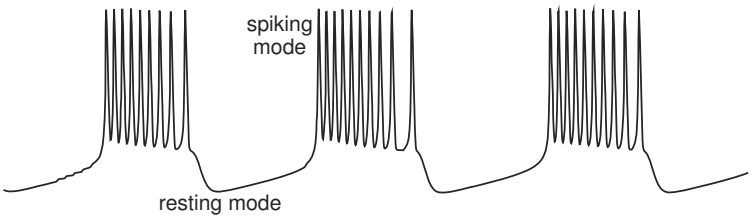

Figure 1.10: Rhythmic transitions between resting and spiking modes result in bursting behavior.

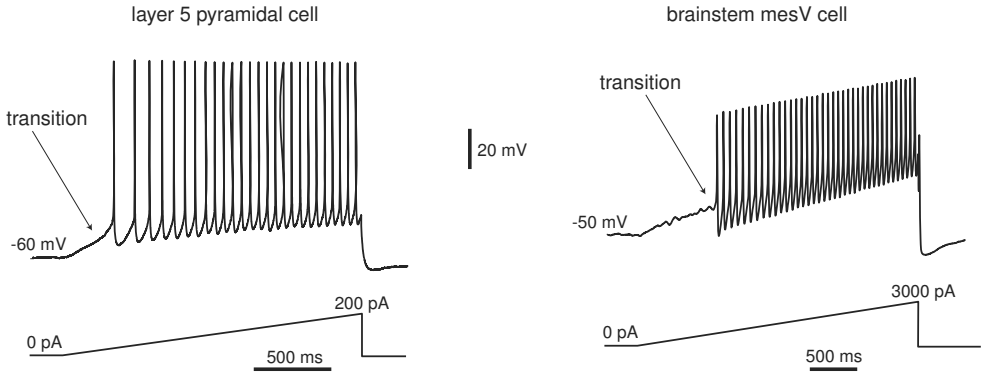

Figure 1.11: As the magnitude of the injected current slowly increases, the neurons bifurcate from resting (equilibrium) mode to tonic spiking (limit cycle) mode.

If we inject a sufficiently strong current into the neuron, we bring it to a pacemaking mode, so that it exhibits periodic spiking activity, as in Fig.1.9c. From the dynamical systems point of view, the state of such a neuron has a stable limit cycle, also known as a stable periodic orbit. The electrophysiological details of the neuron (i.e., the number and the type of currents it has, their kinetics, etc.) determine only the location, the shape, and the period of the limit cycle. As long as the limit cycle exists, the neuron can have periodic spiking activity. Of course, equilibria and limit cycles can coexist, so a neuron can be switched from one mode to another by a transient input. The famous example is the permanent extinguishing of ongoing spiking activity in the squid giant axon by a brief transient depolarizing pulse of current applied at a proper phase (Guttman et al. 1980) – a phenomenon predicted by John Rinzel (1978) purely on the basis of theoretical analysis of the Hodgkin-Huxley model. The transition between resting and spiking modes could be triggered by intrinsic slow conductances, resulting in the bursting behavior in Fig.1.10.

1.2.2 Bifurcations

Now suppose that the magnitude of the injected current is a parameter that we can control, e.g., we can ramp it up, as in Fig.1.11. Each cell in the figure is quiescent at the beginning of the ramps, so its phase portrait has a stable equilibrium and it may look like the one in Fig.1.9a or Fig.1.9b. Then it starts to fire tonic spikes, so its phase portrait has a limit cycle attractor and it may look like the one in Fig.1.9c, with a white circle denoting an unstable resting equilibrium. Apparently there is some intermediate level of injected current that corresponds to the transition from resting to sustained spiking, i.e., from the phase portrait in Fig.1.9b to Fig.1.9c. What does the transition look like?

From the dynamical systems point of view, the transition corresponds to a *bifurcation* of neuron dynamics, i.e., a qualitative change of phase portrait of the system. For example, there is no bifurcation going from the phase portrait in Fig.1.9a to that in Fig.1.9b, since both have one globally stable equilibrium; the difference in behavior is quantitative but not qualitative. In contrast, there is a bifurcation going from Fig.1.9b to Fig.1.9c, since the equilibrium is no longer stable and another attractor, limit cycle, has appeared. The neuron is not excitable in Fig.1.9a but it is in Fig.1.9b, simply because the former phase portrait is far from the bifurcation and the latter is near.

In general, neurons are excitable *because* they are near bifurcations from resting to spiking activity, so the type of the bifurcation determines the excitable properties of the neuron. Of course, the type depends on the neuron's electrophysiology. An amazing observation is that there could be millions of different electrophysiological mechanisms of excitability and spiking, but there are only four – yes, *four* – different types of bifurcations of equilibrium that a system can undergo without any additional constraints, such as symmetry. Thus, considering these four bifurcations in a general setup, we can understand excitable properties of many models, even those that have not been invented yet. What is even more amazing, we can understand excitable properties of neurons whose currents are not measured and whose models are not known, provided we can experimentally identify which of the four bifurcations the resting state of the neuron undergoes.

The four bifurcations are summarized in Fig.1.12, which plots the phase portrait before (left), at (center), and after (right) a particular bifurcation occurs. Mathematicians refer to these bifurcations as being of codimension-1 because we need to vary only one parameter, e.g., the magnitude of the injected DC current I, to observe the bifurcations reliably in simulations or experiments. There are many more codimension-2, 3, (etc.), bifurcations, but they need special conditions to be observed. We discuss these in chapter 6.

Let us consider the four bifurcations and their phase portraits in Fig.1.12. The horizontal and vertical axes are the membrane potential with instantaneous activation variable and a recovery variable, respectively. At this stage, the reader is not required to fully understand the intricacies of the phase portraits in the figure, since they will be explained systematically in later chapters.

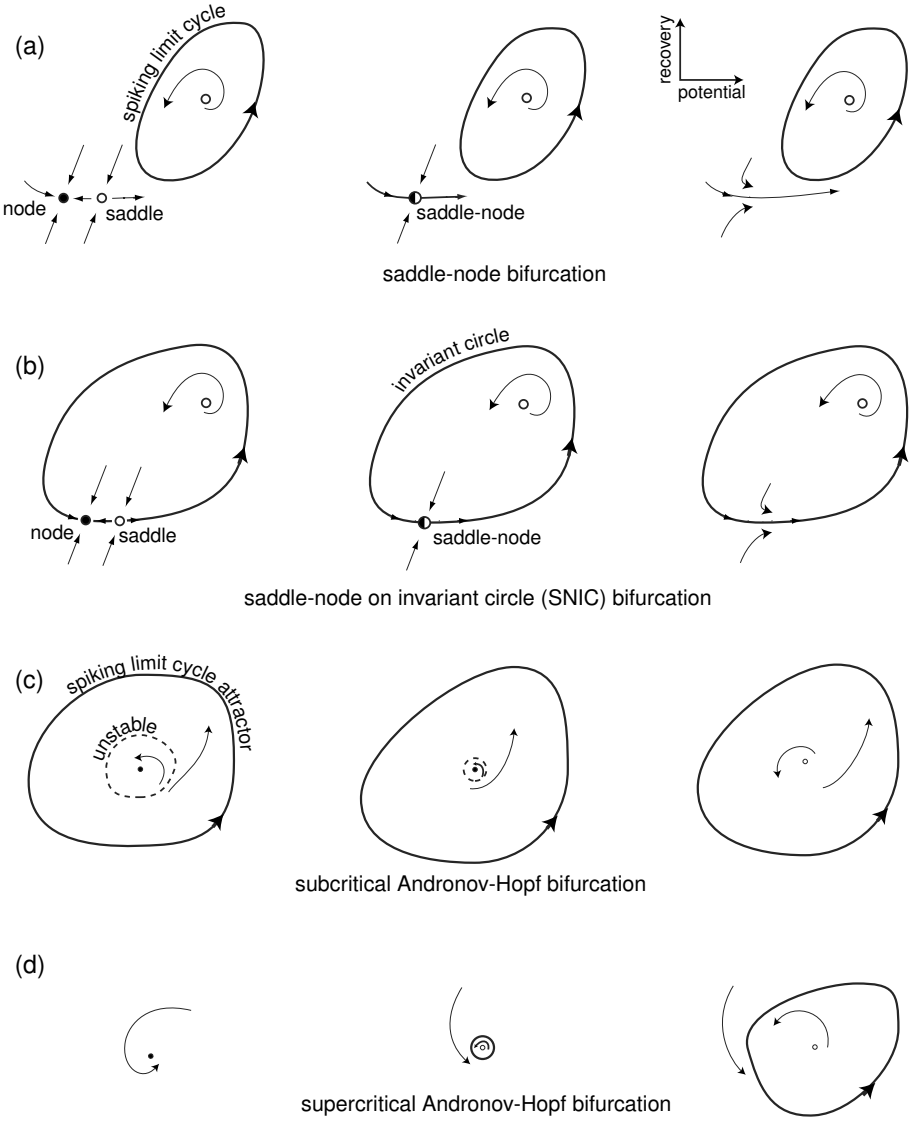

Figure 1.12: Four generic (codimension-1) bifurcations of an equilibrium state leading to the transition from resting to periodic spiking behavior in neurons.

- *Saddle-node bifurcation.* As the magnitude of the injected current or any other bifurcation parameter changes, a stable equilibrium corresponding to the resting state (black circle marked "node" in Fig.1.12a) is approached by an unstable equilibrium (white circle marked "saddle"); they coalesce and annihilate each other, as in Fig.1.12a (middle). Since the resting state no longer exists, the trajectory describing the evolution of the system jumps to the limit cycle attractor, indicating that the neuron starts to fire tonic spikes. Notice that the limit cycle, or some other attractor, must coexist with the resting state in order for the transition resting → spiking to occur.

- *Saddle-node on invariant circle bifurcation* is similar to the saddle-node bifurcation except that there is an invariant circle at the moment of bifurcation, which then becomes a limit cycle attractor, as in Fig.1.12b.

- *Subcritical Andronov-Hopf bifurcation.* A small unstable limit cycle shrinks to a stable equilibrium and makes it lose stability, as in Fig.1.12c. Because of instabilities, the trajectory diverges from the equilibrium and approaches a large-amplitude spiking limit cycle or some other attractor.

- *Supercritical Andronov-Hopf bifurcation.* The stable equilibrium loses stability and gives birth to a small-amplitude limit cycle attractor, as in Fig.1.12d. As the magnitude of the injected current increases, the amplitude of the limit cycle increases and it becomes a full-size spiking limit cycle.

Notice that there is a coexistence of resting and spiking states in the case of saddle-node and subcritical Andronov-Hopf bifurcations, but not in the other two cases. Such a coexistence reveals itself via a hysteresis behavior when the injected current slowly increases and then decreases past the bifurcation value, because the transitions "resting → spiking" and "spiking → resting" occur at different values of the current. In addition, brief stimuli applied at the appropriate times can switch the activity from spiking to resting and back. There are also spontaneous noise-induced transitions between the two modes that result in the stuttering spiking that, for instance, is exhibited by the so-called fast spiking (FS) cortical interneurons when they are kept close to the bifurcation (Tateno et al. 2004). Some bistable neurons have a slow adaptation current that activates during the spiking mode and impedes spiking, often resulting in bursting activity.

Systems undergoing Andronov-Hopf bifurcations, whether subcritical or supercritical, exhibit damped oscillations of membrane potential, whereas systems near saddle-node bifurcations, whether on or off an invariant circle, do not. The existence of small amplitude oscillations creates the possibility of resonance to the frequency of the incoming pulses, as in Fig.1.7, and other interesting features.

We refer to neurons with damped subthreshold oscillations as *resonators* and to those that do not have this property as *integrators*. We refer to the neurons that exhibit the coexistence of resting and spiking states, at least near the transition from

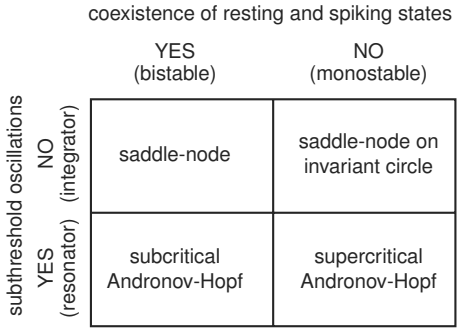

Figure 1.13: Classification of neurons into monostable/bistable integrators/resonators according to the bifurcation of the resting state in Fig.1.12.

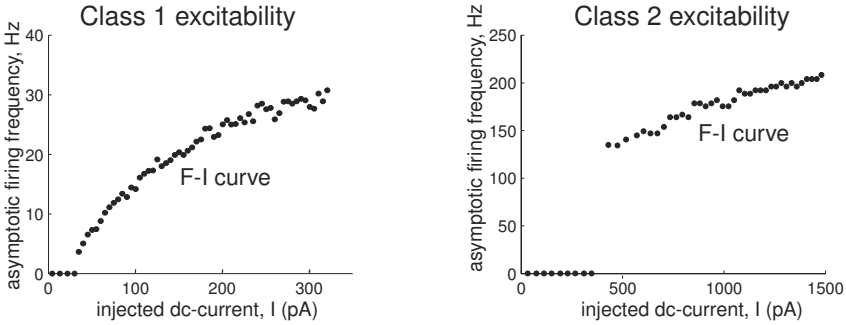

Figure 1.14: Frequency-current (F-I) curves of cortical pyramidal neuron and brainstem mesV neuron from Fig.7.3. These are the same neurons used in the ramp experiment in Fig.1.11.

resting to spiking, as *bistable*, and to those that do not, *monostable*. The four bifurcations in Fig.1.12 are uniquely defined by these two features. For example, a bistable resonator is a neuron undergoing subcritical Andronov-Hopf bifurcation, and a monostable integrator is a neuron undergoing saddle-node on invariant circle bifurcation (see Fig.1.13). Cortical fast spiking (FS) and regular spiking (RS) neurons, studied in chapter 8, are typical examples of the former and the latter, respectively.

1.2.3 Hodgkin Classification

Hodgkin (1948) was the first to study bifurcations in neuronal dynamics, years before the mathematical theory of bifurcations was developed. He stimulated squid axons with pulses of various amplitudes and identified three classes of responses:

- *Class 1 neural excitability.* Action potentials can be generated with arbitrarily low frequency, depending on the strength of the applied current.

- *Class 2 neural excitability.* Action potentials are generated in a certain frequency band that is relatively insensitive to changes in the strength of the applied current.

- *Class 3 neural excitability.* A single action potential is generated in response to a pulse of current. Repetitive (tonic) spiking can be generated only for extremely strong injected currents or not at all.

The qualitative distinction between the classes is that the frequency-current relation (the F-I curve in Fig.1.14) starts from zero and continuously increases for Class 1 neurons, is discontinuous for Class 2 neurons, and is not defined at all for Class 3 neurons.

Obviously, neurons belonging to different classes have different neurocomputational properties. Class 1 neurons, which include cortical excitatory pyramidal neurons, can smoothly encode the strength of the input into the output firing frequency, as in Fig.1.11 (left). In contrast, Class 2 neurons, such as fast-spiking (FS) cortical inhibitory interneurons, cannot do that; instead, they fire in a relatively narrow frequency band, as in Fig.1.11 (right). Class 3 neurons cannot exhibit sustained spiking activity, so Hodgkin regarded them as "sick" or "unhealthy". There are other distinctions between the classes, which we discuss later.

Different classes of excitability occur because neurons have different bifurcations of resting and spiking states – a phenomenon first explained by Rinzel and Ermentrout (1989). If ramps of current are injected to measure the F-I curves, then Class 1 excitability occurs when the neuron undergoes the saddle-node bifurcation on an invariant circle depicted in Fig.1.12b. Indeed, the period of the limit cycle attractor is infinite at the bifurcation point, and then it decreases as the bifurcation parameter – say, the magnitude of the injected current – increases. The other three bifurcations result in Class 2 excitability. Indeed, the limit cycle attractor exists and has a finite period when the resting state in Fig.1.12 undergoes a subcritical Andronov-Hopf bifurcation, so emerging spiking has a nonzero frequency. The period of the small limit cycle attractor appearing via supercritical Andronov-Hopf bifurcation is also finite, so the frequency of oscillations is nonzero, but their amplitudes are small. In contrast to the common and erroneous folklore, the saddle-node bifurcation (off-limit cycle) also results in Class 2 excitability because the limit cycle has a finite period at the bifurcation. There is a considerable latency (delay) to the first spike in this case, but the subsequent spiking has nonzero frequency. Thus, the simple scheme "Class 1 = saddle-node, Class 2 = Hopf" that permeates many publications is unfortunately incorrect.

When pulses of current are used to measure the F-I curve, as in Hodgkin's experiments, the firing frequency depends on factors besides the type of the bifurcation of the resting state. In particular, low-frequency firing can be observed in systems near Andronov-Hopf bifurcations, as we show in chapter 7. To avoid possible confusion, we define the class of excitability only on the basis of slow ramp experiments.

Hodgkin's classification has an important historical value, but it is of little use for the dynamic description of a neuron, since naming a class of excitability of a neuron does not tell much about the bifurcations of the resting state. Indeed, it says only that saddle-node on invariant circle bifurcation (Class 1) is different from the other three bifurcations (Class 2), and only when ramps are injected. Dividing neurons into

integrators and resonators with bistable or monostable activity is more informative, so we adopt the classification in Fig.1.13 in this book. In this classification, a Class 1 neuron is a monostable integrator, whereas a Class 2 neuron can be a bistable integrator or a resonator.

1.2.4 Neurocomputational properties

Using the same arrangement as in Fig.1.13, we depict typical geometry of phase portraits near the four bifurcations in Fig.1.15. Let us use the portraits to explain what happens "near the threshold", i.e., near the place where the decision to fire or not to fire is made. To simplify our geometrical analysis, we assume here that neurons receive shock inputs, i.e., brief but strong pulses of current that do not change the phase portraits, but only push or reset the state of the neuron into various regions of the phase space. We consider these and other cases in detail in chapter 7.

The horizontal axis in each plot in Fig.1.15 corresponds to the membrane potential V with instantaneous Na^+ current, and the vertical axis corresponds to a recovery variable, say activation of K^+ current. Black circles denote stable equilibria corresponding to the neuronal resting state. Spiking limit cycle attractors correspond to sustained spiking states, which exist in the two cases depicted in the left half of the figure corresponding to the bistable dynamics. The limit cycles are surrounded by shaded regions – their attraction domains. The white region is the attraction domain of the equilibrium. To initiate spiking, the external input should push the state of the system into the shaded region, and to extinguish spiking, the input should push the state back into the white region.

There are no limit cycles in the two cases depicted in the right half of the figure, so the entire phase space is the attraction domain of the stable equilibrium, and the dynamics are monostable. However, if the trajectory starts in the shaded region, it makes a large-amplitude rotation before returning to the equilibrium – a transient spike. Apparently, to elicit such a spike, the input should push the state of the system into the shaded region.

Now let us contrast the upper and lower halves of the figure, corresponding to integrators and resonators, respectively. We distinguish these two modes of operation on the basis of the existence of subthreshold oscillations near the equilibrium.

First, let us show that *inhibition impedes spiking in integrators, but can promote it in resonators.* In the integrator, the shaded region is in the depolarized voltage range, i.e., to the right of the equilibrium. Excitatory inputs push the state of the system toward the shaded region, while inhibitory inputs push it away. In resonators, both excitation and inhibition push the state toward the shaded region, because the region wraps around the equilibrium and can be reached along any direction. This explains the rebound spiking phenomenon depicted in Fig.1.6.

Integrators have all-or-none spikes; resonators may not. Indeed, any trajectory starting in the shaded region in the upper half of Fig.1.15 has to rotate around the

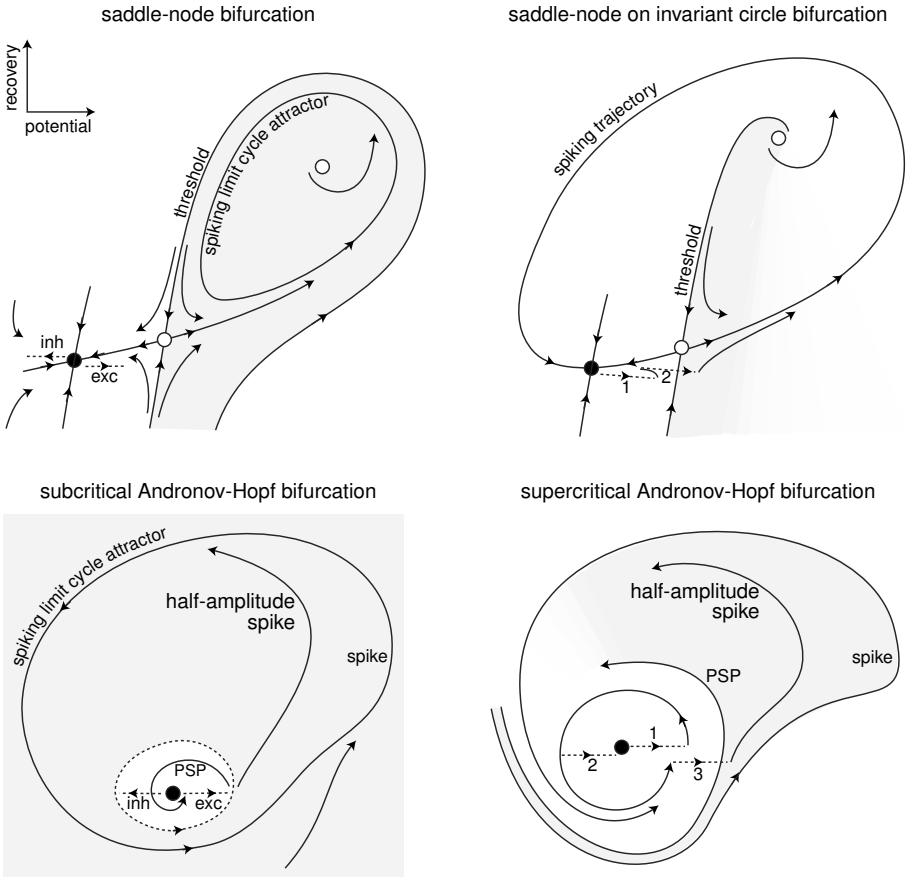

Figure 1.15: The geometry of phase portraits of excitable systems near four bifurcations can explain many neurocomputational properties (see section 1.2.4 for details).

white circle at the top that corresponds to an unstable equilibrium. Moreover, the state of the system is quickly attracted to the spiking trajectory and moves along that trajectory, thereby generating a stereotypical spike. A resonator neuron also can fire large amplitude spikes when its state is pushed to or beyond the trajectory denoted "spike". Such neurons generate subthreshold responses when the state slides along the smaller trajectory denoted PSP; they also can generate spikes of an intermediate amplitude when the state is pushed between the PSP and "spike" trajectories, which explains the partial-amplitude spiking in Fig.1.5b or in the squid axon in Fig.7.26. The set of initial conditions corresponding to such spiking is quite small, so typical spikes have large amplitudes and partial spikes are rare.

Integrators have well-defined thresholds; resonators may not. The white circles near the resting states of integrators in Fig.1.15 are called saddles. They are stable along the

vertical direction and unstable along the horizontal direction. The two trajectories that lead to the saddle along the vertical direction are called separatrices because they separate the phase space into two regions – in this case, white and shaded. The separatrices play the role of thresholds since only those perturbations that push the state of the system beyond them result in a spike. The closer the state of the system is to the separatrices, the longer it takes to converge and then diverge from the saddle, resulting in a long *latency to the spike*. Notice that the threshold is not a point, but a tilted curve that spans a range of voltage values.

Resonators have a well-defined threshold in the case of subcritical Andronov-Hopf bifurcation: it is the small unstable limit cycle that separates the attraction domains of stable equilibrium and spiking limit cycle. Trajectories inside the small cycle spiral toward the stable equilibrium, whereas trajectories outside the cycle spiral away from it and eventually lead to sustained spiking activity. When a neuronal model is far from the subcritical Andronov-Hopf bifurcation, its phase portrait may look similar to the one corresponding to the supercritical Andronov-Hopf bifurcation. The narrow shaded band in the figure is not a threshold manifold but a fuzzy threshold set called "quasi-threshold" by FitzHugh (1955). Many resonators, including the Hodgkin-Huxley model, have quasi-thresholds instead of thresholds. The width of the quasi-threshold in the Hodgkin-Huxley model is so narrow that for all practical reasons it may be assumed to be just a curve.

Integrators integrate, resonators resonate. Now consider inputs consisting of multiple pulses, e.g., a burst of spikes. Integrators prefer high-frequency inputs; the higher the frequency, the sooner they fire. Indeed, the first spike of such an input, marked "1" in the top-right phase portrait in Fig.1.15, increases the membrane potential and shifts the state to the right, toward the threshold. Since the state of the system is still in the white area, it slowly converges back to the stable equilibrium. To cross the threshold manifold, the second pulse must arrive shortly after the first one. The reaction of a resonator to a pair of pulses is quite different. The first pulse initiates a damped subthreshold oscillation of the membrane potential, which looks like a spiral in the bottom-right phase portrait in Fig.1.15. The effect of the second pulse depends on its timing. If it arrives after the trajectory makes half a rotation, marked "2" in the figure, it cancels the effect of the first pulse. If it arrives after the trajectory makes a full rotation, marked "3" in the figure, it adds to the first pulse and either increases the amplitude of subthreshold oscillation or evokes a spike response. Thus, the response of the resonator neuron depends on the frequency content of the input, as in Fig.1.7.

Integrators and resonators constitute two major modes of activity of neurons. Most cortical pyramidal neurons, including the regular spiking (RS), intrinsically bursting (IB), and chattering (CH) types considered in Chap. 8, are integrators. So are thalamocortical neurons in the relay mode of firing, and neostriatal spiny projection neurons. Most cortical inhibitory interneurons, including the FS type, are resonators. So are brainstem mesencephalic V neurons and stellate neurons of the entorhinal cortex. Some cortical pyramidal neurons and low-threshold spiking (LTS) interneurons can be at the border of transition between integrator and resonator modes. Such a transition corre-

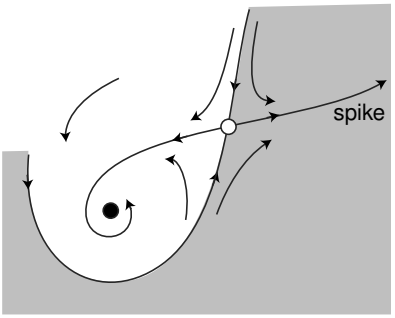

Figure 1.16: Phase portrait of a system near a Bogdanov-Takens bifurcation that corresponds to the transition from integrator to resonator mode.

sponds to another bifurcation, which has codimension-2, and hence it is less likely to be encountered experimentally. We consider this and other uncommon bifurcations in detail later. The phase portrait near the bifurcation is depicted in Fig.1.16, and it is a good exercise for the reader to explain why such a system has damped oscillations and postinhibitory responses, yet a well-defined threshold, all-or-none spikes, and possibly long latencies.

Of course, figures 1.15 and 1.16 cannot encompass all the richness of neuronal behavior, otherwise this book would be only 19pages long (this book is actually quite short; most of the space is taken by figures, exercises, and solutions). Many aspects of neuronal dynamics depend on other bifurcations, e.g., those corresponding to appearance and disappearance of spiking limit cycles. These bifurcations describe the transitions from spiking to resting, and they are especially important when we consider bursting activity. In addition, we need to take into account the relative geometry of equilibria, limit cycles, and other relevant trajectories, and how they depend on the parameters of the system, such as maximal conductances, and activation time constants. We explore all these issues systematically in subsequent chapters.

In chapter 2 we review some of the most fundamental concepts of neuron electrophysiology, culminating with the Hodgkin-Huxley model. This chapter is aimed at mathematicians learning neuroscience. In chapters 3 and 4 we use one- and two-dimensional neuronal models, respectively, to review some of the most fundamental concepts of dynamical systems, such as equilibria, limit cycles, stability, attraction domain, nullclines, phase portrait, and bifurcation. The material in these chapters, aimed at biologists learning the language of dynamical systems, is presented with the emphasis on geometrical rather than mathematical intuition. In fact, the spirit of the entire book is to explain concepts by using pictures, not equations. Chapter 5 explores phase portraits of various conductance-based models and the relations between ionic currents and dynamic behavior. In Chapter 6 we use the $I_{\mathrm{Na,p}}$+I_{K}-model to systematically introduce the geometric bifurcation theory. Chapter 7, probably the most important chapter of the book, applies the theory to explain many computational properties of neurons. In fact, all the material in the previous chapters is given so that the reader can understand this chapter. In chapter 8 we use a simple phenomenological

model to simulate many cortical, hippocampal, and thalamic neurons. This chapter contains probably the most comprehensive up-to-date review of various firing patterns exhibited by mammalian neurons. In chapter 9 we introduce the electrophysiological and topological classification of bursting dynamics, as well as some useful methods to study the bursters. Finally, the last and the most mathematically advanced chapter of the book, Chap. 10, deals with coupled neurons. There we show how the details of the spike generation mechanism of neurons affect neurons' collective properties, such as synchronization.

1.2.5 Building Models (Revisited)

To have a good model of a neuron, it is not enough to put the right kind of currents together and tune the parameters so that the model can fire spikes. It is not even enough to reproduce the right input resistance, rheobase, and firing frequencies. The model has to reproduce all the neurocomputational features of the neuron, starting with the coexistence of resting and spiking states, spike latencies, subthreshold oscillations, and rebound spikes, among others.

A good way to start is to determine what kind of bifurcations the neuron under consideration undergoes and how the bifurcations depend on neuromodulators and pharmacological blockers. Instead of or in addition to measuring neuronal responses to get the kinetic parameters, we need to measure them to get the right bifurcation behavior. Only in this case we can be sure that the behavior of the model is *equivalent* to that of the neuron, even if we omitted a current or guessed some of the parameters incorrectly.

Implementation of this research program is still a pipe dream. The people who understand the mathematical aspects of neuron dynamics – those who see beyond conductances and currents – usually do not have the opportunity to do experiments. Conversely, those who study neurons in vitro or in vivo on a daily basis – those who see spiking, bursting, and oscillations; those who can manipulate the experimental setup to test practically any aspect of neuronal activity – do not usually see the value of studying phase portraits, bifurcations, and nonlinear dynamics in general. One of the goals of this book is to change this state and bring these two groups of people closer together.

Review of Important Concepts

- Neurons are dynamical systems.
- The resting state of neurons corresponds to a stable equilibrium; the tonic spiking state corresponds to a limit cycle attractor.
- Neurons are excitable because the equilibrium is near a bifurcation.
- There are many ionic mechanisms of spike generation, but only four generic bifurcations of equilibria.
- These bifurcations divide neurons into four categories: integrators or resonators, monostable or bistable.
- Analyses of phase portraits at bifurcations explain why some neurons have well-defined thresholds, all-or-none spikes, postinhibitory spikes, frequency preference, hysteresis, and so on, while others do not.
- These features, and not ionic currents per se, determine the neuronal responses, i.e., the kind of computations neurons do.
- A good neuronal model must reproduce not only electrophysiology but also the bifurcation dynamics of neurons.

Bibliographical Notes

Richard FitzHugh at the National Institutes of Health (NIH) pioneered the phase plane analysis of neuronal models with the view to understanding their neurocomputational properties. He was the first to analyze the Hodgkin-Huxley model (FitzHugh 1955; years before they received the Nobel Prize) and to prove that it has neither threshold nor all-or-none spikes. FitzHugh (1961) introduced the simplified model of excitability (see Fig.1.18) and showed that one can get the right kind of neuronal dynamics in models lacking conductances and currents. Nagumo et al. (1962) designed a corresponding tunnel diode circuit, so the model is called the FitzHugh-Nagumo oscillator. Chapter 8 deals with such simplified models. The history of the development of FitzHugh-Nagumo model is reviewed by Izhikevich and FitzHugh (2006).

FitzHugh's research program was further developed by John Rinzel and G. Bard Ermentrout (see Fig.1.19 and Fig.1.20). In their 1989 seminal paper, Rinzel and Ermentrout revived Hodgkin's classification of excitability and pointed out the connection between the behavior of neuronal models and the bifurcations they exhibit. (They also referred to the excitability as "type I" or "type II"). Unfortunately, many people treat

Figure 1.17: Richard FitzHugh in 1984.

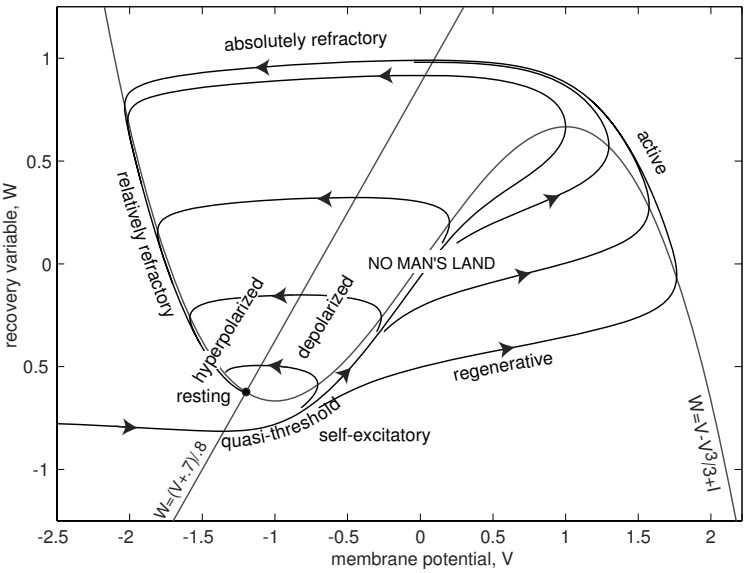

Figure 1.18: Phase portrait and physiological state diagram of FitzHugh-Nagumo model $\dot{V} = V - V^3/3 - W + I$, $\dot{W} = 0.08(V + 0.7 - 0.8W)$. The meaning of curves and trajectories is explained in chapter 4. (Reproduced from Izhikevich and FitzHugh (2006) with permission.)

Figure 1.19: John Rinzel in 2004. Depicted on his T-shirt is the cover of the first issue of *Journal of Computational Neuroscience*, in which the Pinsky-Rinzel (1994) model appeared.

Figure 1.20: G. Bard Ermentrout (G. stands for George) with his parrot, Junior, in 1983.

the connection in a simpleminded fashion and incorrectly identify "type I = saddle-node, type II = Hopf". If only life were so simple!

The geometrical analysis of neuronal models was further developed by, among others, Izhikevich (2000a), who stressed the integrator and resonator modes of operation and made connections to other neurocomputational properties.

The neuroscience and mathematics parts of this book are standard, though many connections are new. The literature sources are listed at the end of each chapter. Among many outstanding books on computational neuroscience, the author especially recommends *Spikes, Decisions, and Actions* by Wilson (1999), *Biophysics of Computation* by Koch (1999), *Theoretical Neuroscience* by Dayan and Abbott (2001), and *Foundations of Cellular Neurophysiology* by Johnston and Wu (1995). The present volume complements these excellent books in the sense that it is more ambitious, focused, and thorough in dealing with neurons as dynamical systems. Though its views may be biased by the author's philosophy and taste, the payoffs in understanding neuronal dynamics are immense, provided the reader has enough patience and perseverance to follow the author's line of thought.

The NEURON simulation environment is described by Hines (1989) and Carnevale and Hines (2006) (`http://www.neuron.yale.edu`); the GENESIS environment, by Bower and Beeman (1995) (`http://www.genesis-sim.org`); the XPP environment, by Ermentrout (2002). The author of this book uses MATLAB, which has become a standard computational tool in science and engineering. MATLAB is the registered trademark of The MathWorks, Inc. (`http://www.mathworks.com`).

Chapter 2

Electrophysiology of Neurons

In this chapter we remind the reader of some fundamental concepts of neuronal electrophysiology that are necessary to understand the rest of the book. We start with ions and currents, and move quickly toward the dynamics of the Hodgkin-Huxley model. If the reader is already familiar with the Hodgkin-Huxley formalism, this chapter can be skipped. Our exposition is brief, and it cannot substitute for a good introductory neuroscience course or the reading of such excellent textbooks as *Theoretical Neuroscience* by Dayan and Abbott (2001), *Foundations of Cellular Neurophysiology* by Johnston and Wu (1995), *Biophysics of Computation* by Koch (1999), or *Ion Channels of Excitable Membranes* by Hille (2001).

2.1 Ions

Electrical activity in neurons is sustained and propagated via ionic currents through neuron membranes. Most of these transmembrane currents involve one of four ionic species: sodium (Na^+), potassium (K^+), calcium (Ca^{2+}), or chloride (Cl^-). The first three have a positive charge (cations) and the fourth has a negative charge (anion). The concentrations of these ions are different on the inside and the outside of a cell, which creates electrochemical gradients – the major driving forces of neural activity. The extracellular medium has a high concentration of Na^+ and Cl^- (salty, like seawater) and a relatively high concentration of Ca^{2+}. The intracellular medium has high concentrations of K^+ and negatively charged molecules (denoted by A^-), as we illustrate in Fig.2.1.

The cell membrane has large protein molecules forming channels through which ions (but not A^-) can flow according to their electrochemical gradients. The flow of Na^+ and Ca^{2+} ions is not significant, at least at rest, but the flow of K^+ and Cl^- ions is. This, however, does not eliminate the concentration asymmetry for two reasons.

- *Passive redistribution.* The impermeable anions A^- attract more K^+ into the cell (opposites attract) and repel more Cl^- out of the cell, thereby creating concentration gradients.
- *Active transport.* Ions are pumped in and out of the cell via ionic pumps. For example, the Na^+-K^+ pump depicted in Fig.2.1 pumps out three Na^+ ions for every two K^+ ions pumped in, thereby maintaining concentration gradients.

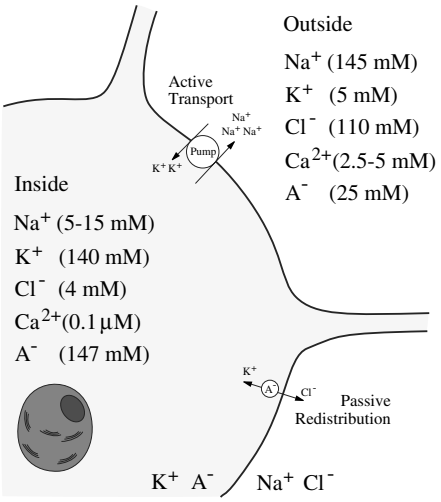

Equilibrium Potentials

$$\begin{aligned}
\mathrm{Na}^+ \quad & 62 \log \tfrac{145}{5} = 90 \text{ mV} \\
& 62 \log \tfrac{145}{15} = 61 \text{ mV} \\
\mathrm{K}^+ \quad & 62 \log \tfrac{5}{140} = -90 \text{ mV} \\
\mathrm{Cl}^- \quad & -62 \log \tfrac{110}{4} = -89 \text{ mV} \\
\mathrm{Ca}^{2+} \quad & 31 \log \tfrac{2.5}{10^{-4}} = 136 \text{ mV} \\
& 31 \log \tfrac{5}{10^{-4}} = 146 \text{ mV}
\end{aligned}$$

Figure 2.1: Ion concentrations and Nernst equilibrium potentials (2.1) in a typical mammalian neuron (modified from Johnston and Wu 1995). A^- are membrane-impermeant anions. Temperature $T = 37°\mathrm{C}$ (310°K).

2.1.1 Nernst Potential

There are two forces that drive each ion species through the membrane channel: concentration and electric potential gradients. First, the ions diffuse down the concentration gradient. For example, the K^+ ions depicted in Fig.2.2a diffuse out of the cell because K^+ concentration inside is higher than that outside. While exiting the cell, K^+ ions carry a positive charge and leave a net negative charge inside the cell (consisting mostly of impermeable anions A^-), thereby producing the outward current. The positive and negative charges accumulate on the opposite sides of the membrane surface, creating an electric potential gradient across the membrane – *transmembrane potential* or *membrane voltage*. This potential slows the diffusion of K^+, since K^+ ions are attracted to the negatively charged interior and repelled from the positively charged exterior of the membrane, as we illustrate in Fig.2.2b. At some point an equilibrium is achieved: the concentration gradient and the electric potential gradient exert equal and opposite forces that counterbalance each other, and the net cross-membrane current is zero, as in Fig.2.2c. The value of such an *equilibrium potential* depends on the ionic species, and it is given by the Nernst equation (Hille 2001):

$$E_{\text{ion}} = \frac{RT}{zF} \ln \frac{[\text{Ion}]_{\text{out}}}{[\text{Ion}]_{\text{in}}} , \tag{2.1}$$

where $[\text{Ion}]_{\text{in}}$ and $[\text{Ion}]_{\text{out}}$ are concentrations of the ions inside and outside the cell, respectively; R is the universal gas constant ($8,315$ mJ/(K°·Mol)); T is temperature in degrees Kelvin (K° = 273.16+C°); F is Faraday's constant ($96,480$ coulombs/Mol),

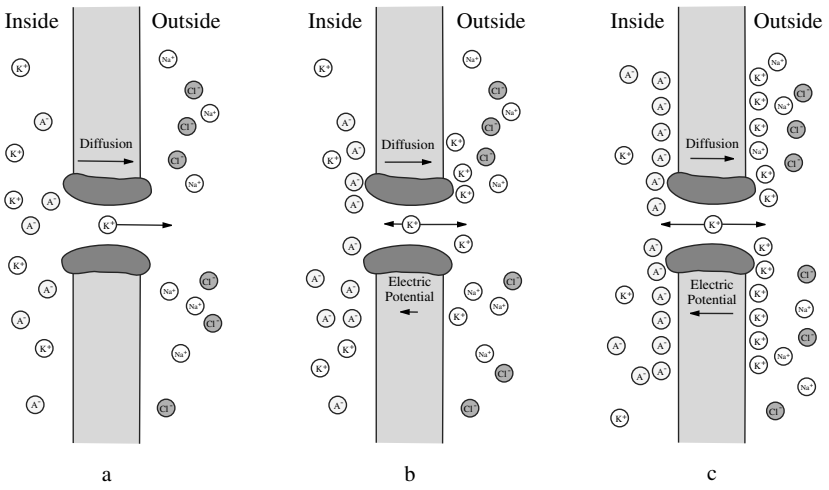

Figure 2.2: Diffusion of K^+ ions down the concentration gradient though the membrane (a) creates an electric potential force pointing in the opposite direction (b) until the diffusion and electrical forces counter each other (c). The resulting transmembrane potential (2.1) is referred to as the Nernst equilibrium potential for K^+.

z is the valence of the ion ($z = 1$ for Na^+ and K^+; $z = -1$ for Cl^-; and $z = 2$ for Ca^{2+}). Substituting the numbers, taking $\log_{10}$ instead of natural ln and using body temperature $T = 310°K$ (37°C) results in

$$E_{\text{ion}} \approx 62 \log \frac{[\text{Ion}]_{\text{out}}}{[\text{Ion}]_{\text{in}}} \quad (\text{mV})$$

for monovalent ($z = 1$) ions. Nernst equilibrium potentials in a typical mammalian neuron are summarized in Fig.2.1.

2.1.2 Ionic Currents and Conductances

In the rest of the book V denotes the membrane potential and E_{Na}, E_{Ca}, E_{K}, and E_{Cl} denote the Nernst equilibrium potentials. When the membrane potential equals the equilibrium potential, say E_{K}, the net K^+ current, denoted as I_{K} ($\mu A/cm^2$), is zero (this is the definition of the Nernst equilibrium potential for K^+). Otherwise, the net K^+ current is proportional to the difference of potentials; that is,

$$I_{\text{K}} = g_{\text{K}} (V - E_{\text{K}}) ,$$

where the positive parameter g_{K} (mS/cm^2) is the K^+ conductance and $(V - E_{\text{K}})$ is the K^+ *driving force.* The other major ionic currents,

$$I_{\text{Na}} = g_{\text{Na}} (V - E_{\text{Na}}) , \qquad I_{\text{Ca}} = g_{\text{Ca}} (V - E_{\text{Ca}}) , \qquad I_{\text{Cl}} = g_{\text{Cl}} (V - E_{\text{Cl}}) ,$$

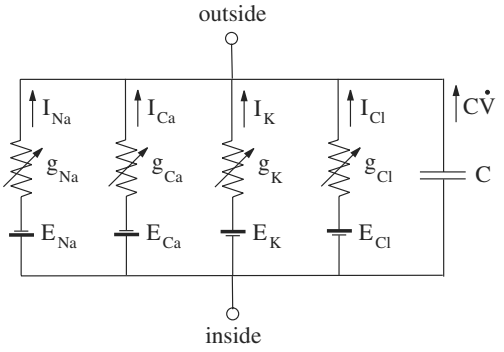

Figure 2.3: Equivalent circuit representation of a patch of cell membrane.

could also be expressed as products of nonlinear conductances and corresponding driving forces. A better description of membrane currents, especially Ca^{2+} current, is provided by the Goldman-Hodgkin-Katz equation (Hille 2001), which we do not use in this book.

When the conductance is constant, the current is said to be *Ohmic*. In general, ionic currents in neurons are not Ohmic, since the conductances may depend on time, membrane potential, and pharmacological agents, e.g., neurotransmitters, neuromodulators, second-messengers, etc. It is the time-dependent variation in conductances that allows a neuron to generate an action potential, or spike.

2.1.3 Equivalent Circuit

It is traditional to represent electrical properties of membranes in terms of equivalent circuits similar to the one depicted in Fig.2.3. According to Kirchhoff's law, the total current, I, flowing across a patch of a cell membrane is the sum of the membrane capacitive current $C\dot{V}$ (the capacitance $C \approx 1.0\,\mu\mathrm{F/cm^2}$ in the squid axon) and all the ionic currents

$$I = C\dot{V} + I_{\mathrm{Na}} + I_{\mathrm{Ca}} + I_{\mathrm{K}} + I_{\mathrm{Cl}} \,,$$

where $\dot{V} = dV/dt$ is the derivative of the voltage variable V with respect to time t. The derivative arises because it takes time to charge the membrane. This is the first *dynamic* term in the book! We write this equation in the standard "dynamical system" form

$$C\dot{V} = I - I_{\mathrm{Na}} - I_{\mathrm{Ca}} - I_{\mathrm{K}} - I_{\mathrm{Cl}} \tag{2.2}$$

or

$$C\dot{V} = I - g_{\mathrm{Na}}\,(V - E_{\mathrm{Na}}) - g_{\mathrm{Ca}}\,(V - E_{\mathrm{Ca}}) - g_{\mathrm{K}}\,(V - E_{\mathrm{K}}) - g_{\mathrm{Cl}}\,(V - E_{\mathrm{Cl}}) \,. \tag{2.3}$$

If there are no additional current sources or sinks, such as synaptic current, axial current, or tangential current along the membrane surface, or current injected via an

electrode, then $I = 0$. In this case, the membrane potential is typically bounded by the equilibrium potentials in the order (see Fig.2.4)

$$E_{\rm K} < E_{\rm Cl} < V_{\rm (at\ rest)} < E_{\rm Na} < E_{\rm Ca}\ ,$$

so that $I_{\rm Na}, I_{\rm Ca} < 0$ (inward currents) and $I_{\rm K}, I_{\rm Cl} > 0$ (outward currents). From (2.2) it follows that inward currents increase the membrane potential, that is, make it more positive (depolarization), whereas outward currents decrease it, that is, make it more negative (hyperpolarization). Note that $I_{\rm Cl}$ is called an outward current even though the flow of Cl^- ions is inward; the ions bring negative charge inside the membrane, which is equivalent to positively charged ions leaving the cell, as in $I_{\rm K}$.

2.1.4 Resting Potential and Input Resistance

If there were only K^+ channels, as in Fig.2.2, the membrane potential would quickly approach the K^+ equilibrium potential, $E_{\rm K}$, which is around -90 mV. Indeed,

$$C\,\dot{V} = -I_{\rm K} = -g_{\rm K}(V - E_{\rm K})$$

in this case. However, most membranes contain a diversity of channels. For example, Na^+ channels would produce an inward current and pull the membrane potential toward the Na^+ equilibrium potential, $E_{\rm Na}$, which could be as large as $+90$ mV. The value of the membrane potential at which all inward and outward currents balance each other so that the net membrane current is zero corresponds to the *resting membrane potential*. It can be found from (2.3) with $I = 0$, by setting $\dot{V} = 0$. The resulting expression,

$$V_{\rm rest} = \frac{g_{\rm Na}E_{\rm Na} + g_{\rm Ca}E_{\rm Ca} + g_{\rm K}E_{\rm K} + g_{\rm Cl}E_{\rm Cl}}{g_{\rm Na} + g_{\rm Ca} + g_{\rm K} + g_{\rm Cl}} \tag{2.4}$$

has a nice mechanistic interpretation: $V_{\rm rest}$ is the center of mass of the balance depicted in Fig.2.4. Incidentally, the entire equation (2.3) can be written in the form

$$C\,\dot{V} = I - g_{\rm inp}(V - V_{\rm rest})\ , \tag{2.5}$$

where

$$g_{\rm inp} = g_{\rm Na} + g_{\rm Ca} + g_{\rm K} + g_{\rm Cl}$$

is the total membrane conductance, called *input conductance*. The quantity $R_{\rm inp} = 1/g_{\rm inp}$ is the *input resistance* of the membrane, and it measures the asymptotic sensitivity of the membrane potential to injected or intrinsic currents. Indeed, from (2.5) it follows that

$$V \to V_{\rm rest} + IR_{\rm inp}\ , \tag{2.6}$$

so greater values of $R_{\rm inp}$ imply greater steady-state displacement of V due to the injection of DC current I.

A remarkable property of neuronal membranes is that ionic conductances, and hence the input resistance, are functions of V and time. We can use (2.6) to trace an action

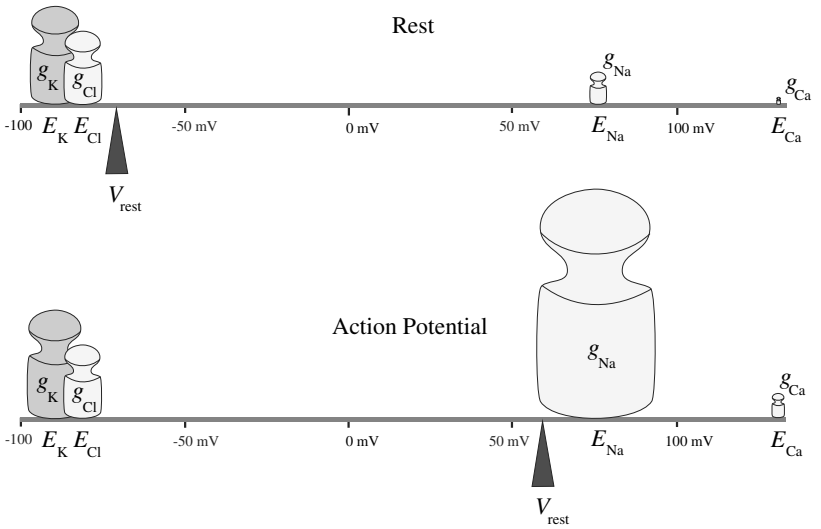

Figure 2.4: Mechanistic interpretation of the resting membrane potential (2.4) as the center of mass. Na^+ conductance increases during the action potential.

potential in a quasi-static fashion, i.e., assuming that time is frozen. When a neuron is quiescent, Na^+ and Ca^{2+} conductances are relatively small, V_{rest} is near E_{K} and E_{Cl}, as in Fig.2.4 (top), and so is V. During the upstroke of an action potential, the Na^+ or Ca^{2+} conductance becomes very large; V_{rest} is near E_{Na}, as in Fig.2.4 (bottom), and V increases, trying to catch V_{rest}. This event is, however, quite brief, for the reasons explained in subsequent sections.

2.1.5 Voltage-Clamp and I-V Relation

In section 2.2 we will study how the membrane potential affects ionic conductances and currents, assuming that the potential is fixed at certain value V_{c} controlled by an experimenter. To maintain the membrane potential constant (clamped), one inserts a metallic conductor to short-circuit currents along the membrane (space-clamp), and then injects a current proportional to the difference $V_{\text{c}} - V$ (voltage-clamp), as in Fig.2.5. From (2.2) and the clamp condition $\dot{V} = 0$, it follows that the injected current I equals the net current generated by the membrane conductances.

In a typical voltage-clamp experiment the membrane potential is held at a certain resting value V_{c} and then reset to a new value V_{s}, as in Fig.2.6a. The injected membrane current needed to stabilize the potential at the new value is a function of time, the pre-step holding potential V_{c}, and the step potential V_{s}. First, the current jumps to a new value to accommodate the instantaneous voltage change from V_{c} to V_{s}. From (2.5) we find that the amplitude of the jump is $g_{\text{inp}}(V_{\text{s}} - V_{\text{c}})$. Then, time- and voltage-

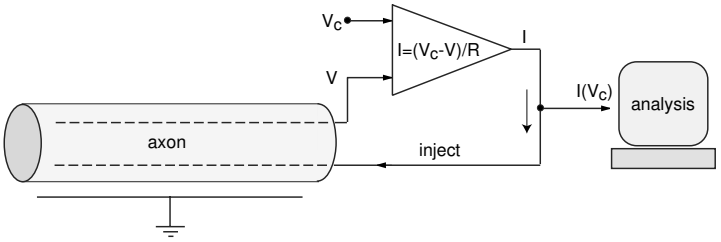

Figure 2.5: Two-wire voltage-clamp experiment on the axon. The top wire is used to monitor the membrane potential V. The bottom wire is used to inject the current I, proportional to the difference $V_c - V$, to keep the membrane potential at V_c.

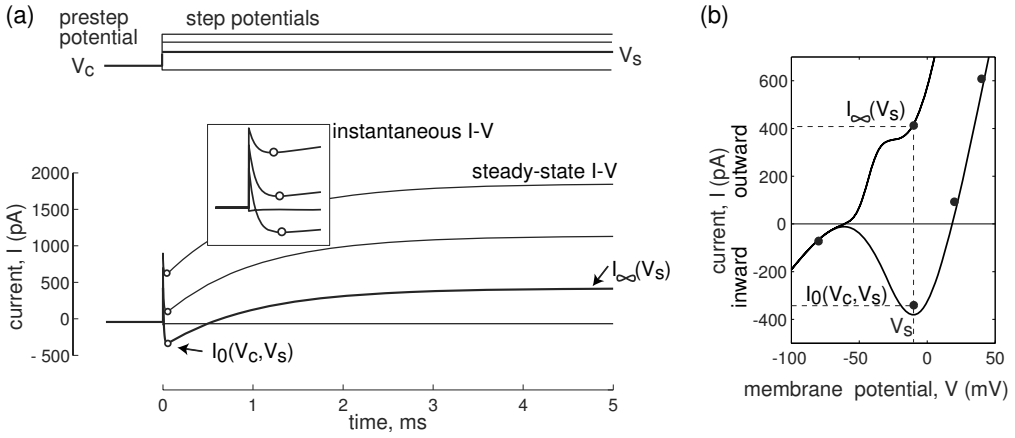

Figure 2.6: Voltage-clamp experiment to measure instantaneous and steady-state I-V relation. Shown are simulations of the $I_{\rm Na}$+$I_{\rm K}$-model (see Fig.4.1b); the continuous curves are theoretically found I-V relations.

dependent processes start to occur and the current decreases and then increases. The value at the negative peak, marked by the open circle "o" in Fig.2.6, depends only on V_c and V_s, and it is called *the instantaneous current-voltage (I-V) relation*, or $I_0(V_c, V_s)$. The asymptotic ($t \to \infty$) value depends only on V_s and it is called the *steady-state current-voltage (I-V) relation*, or $I_\infty(V_s)$.

Both relations, depicted in Fig.2.6b, can be found experimentally (black circles) or theoretically (curves). The instantaneous I-V relation usually has a non-monotone N-shape reflecting nonlinear autocatalytic (positive feedback) transmembrane processes, which are fast enough on the time scale of the action potential that they can be assumed to have instantaneous kinetics. The steady-state I-V relation measures the asymptotic values of all transmembrane processes, and it may be monotone (as in the figure) or not, depending on the properties of the membrane currents. Both I-V relations provide invaluable quantitative information about the currents operating on fast and slow time

Figure 2.7: To tease out neuronal currents, biologists employ an arsenal of sophisticated "clamp" methods, such as current-, voltage-, conductance-, and dynamic-clamp.

scales, and both are useful in building mathematical models of neurons. Finally, when $I_\infty(V) = 0$, the net membrane current is zero, and the potential is at rest or equilibrium, which may still be unstable, as we discuss in the next chapter.

2.2 Conductances

Ionic channels are large transmembrane proteins having aqueous pores through which ions can flow down their electrochemical gradients. The electrical conductance of individual channels may be controlled by gating particles (gates), which switch the channels between open and closed states. The gates may be sensitive to the following factors:

- *Membrane potential.* Example: voltage-gated Na^+ or K^+ channels
- *Intracellular agents* (second-messengers). Example: Ca^{2+}-gated K^+ channels
- *Extracellular agents* (neurotransmitters and neuromodulators). Examples: AMPA, NMDA, or GABA receptors.

Despite the stochastic nature of transitions between open and closed states in individual channels, the net current generated by a large population or ensemble of identical channels can reasonably be described by the equation

$$I = \bar{g}\, p\, (V - E)\ , \tag{2.7}$$

where p is the average proportion of channels in the open state, $\bar{g}$ is the *maximal conductance* of the population, and E is the *reverse potential* of the current, i.e., the potential at which the current reverses its direction. If the channels are selective

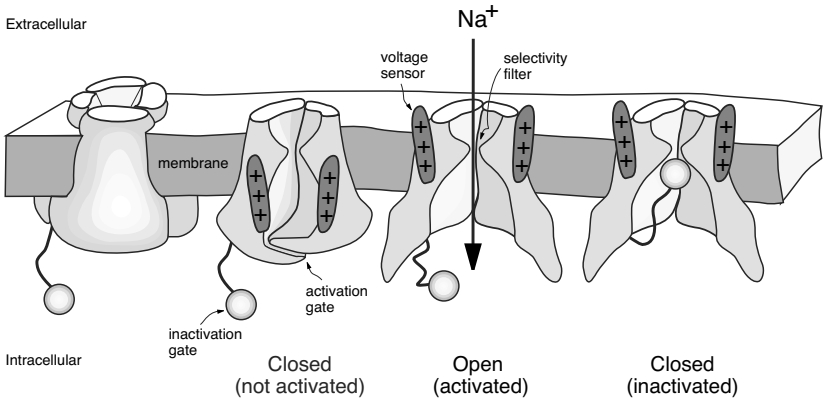

Figure 2.8: Structure of voltage-gated ion channels. Voltage sensors open an activation gate and allow selected ions to flow through the channel according to their electrochemical gradients. The inactivation gate blocks the channel. (Modified from Armstrong and Hille 1998.)

for a single ionic species, then the reverse potential E equals the Nernst equilibrium potential (2.1) for that ionic species (see exercise 2).

2.2.1 Voltage-Gated Channels

When the gating particles are sensitive to the membrane potential, the channels are said to be *voltage-gated*. The gates are divided into two types: those that *activate* or open the channels, and those that *inactivate* or close them (see Fig.2.8). According to the tradition initiated in the middle of the twentieth century by Hodgkin and Huxley, the probability of an activation gate being in the open state is denoted by the variable m (sometimes the variable n is used for K^+ and Cl^- channels). The probability of an inactivation gate being in the open state is denoted by the variable h. The proportion of open channels in a large population is

$$p = m^a \, h^b \, , \tag{2.8}$$

where a is the number of activation gates and b is the number of inactivation gates per channel. The channels can be partially ($0 < m < 1$) or completely *activated* ($m = 1$); not activated or *deactivated* ($m = 0$); *inactivated* ($h = 0$); released from inactivation or *deinactivated* ($h = 1$). Some channels do not have inactivation gates ($b = 0$), hence $p = m^a$. Such channels do not inactivate, and they result in *persistent* currents. In contrast, channels that do inactivate result in *transient* currents.

Below we describe voltage- and time-dependent kinetics of gates. This description is often referred to as the *Hodgkin-Huxley gate model* of membrane channels.

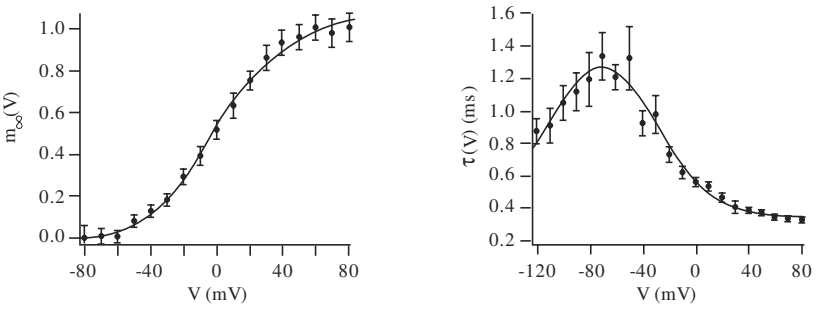

Figure 2.9: The activation function $m_\infty(V)$ and the time constant $\tau(V)$ of the fast transient K^+ current in layer 5 neocortical pyramidal neurons. (Modified from Korngreen and Sakmann 2000.)

2.2.2 Activation of Persistent Currents

The dynamics of the activation variable m is described by the first-order differential equation

$$\dot{m} = (m_\infty(V) - m)/\tau(V) \,, \tag{2.9}$$

where the voltage-sensitive steady-state *activation function* $m_\infty(V)$ and the *time constant* $\tau(V)$ can be measured experimentally. They have sigmoid and unimodal shapes, respectively, as in Fig.2.9 (see also Fig.2.20). The steady-state activation function $m_\infty(V)$ gives the asymptotic value of m when the potential is fixed (voltage-clamp). Smaller values of $\tau(V)$ result in faster dynamics of m.

In Fig.2.10 we depict a typical experiment to determine $m_\infty(V)$ of a persistent current, i.e., a current having no inactivation variable. Initially we hold the membrane potential at a hyperpolarized value V_0 so that all activation gates are closed and $I \approx 0$. Then we step-increase V to a greater value V_s ($s = 1, \ldots, 7$; see Fig.2.10a) and hold it there until the current is essentially equal to its asymptotic value, which is denoted here as I_s (s stands for "step"; see Fig.2.10b). Repeating the experiment for various stepping potentials V_s, one can easily determine the corresponding I_s, and hence the entire steady-state I-V relation, which we depict in Fig.2.10c. According to (2.7), $I(V) = \bar{g} m_\infty(V)(V - E)$, and the steady-state activation curve $m_\infty(V)$ depicted in Fig.2.10d is $I(V)$ divided by the driving force $(V - E)$ and normalized so that $\max m_\infty(V) = 1$. To determine the time constant $\tau(V)$, one needs to analyze the convergence rates. In exercise 6 we describe an efficient method to determine $m_\infty(V)$ and $\tau(V)$.

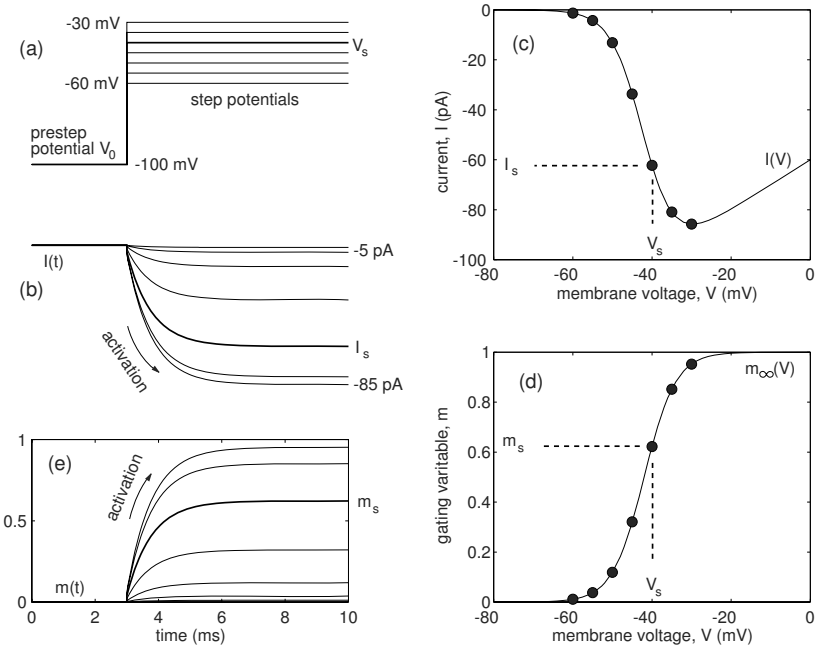

Figure 2.10: An experiment to determine $m_\infty(V)$. Shown are simulations of the persistent Na^+ current in Purkinje cells (see section 2.3.5).

2.2.3 Inactivation of Transient Currents

The dynamics of the inactivation variable h can be described by the first-order differential equation

$$\dot{h} = (h_\infty(V) - h)/\tau(V) \;, \tag{2.10}$$

where $h_\infty(V)$ is the voltage-sensitive steady-state *inactivation function* depicted in Fig.2.11. In Fig.2.12 we present a typical voltage-clamp experiment to determine $h_\infty(V)$ in the presence of activation $m_\infty(V)$. It relies on the observation that inactivation kinetics is usually slower than activation kinetics. First, we hold the membrane potential at a certain pre-step potential V_s for a long enough time that the activation and inactivation variables are essentially equal to their steady-state values $m_\infty(V_s)$ and $h_\infty(V_s)$, respectively, which have yet to be determined. Then we step-increase V to a sufficiently high value V_0, chosen so that $m_\infty(V_0) \approx 1$. If activation is much faster than inactivation, m approaches 1 after the first few milliseconds, while h continues to be near its asymptotic value $h_s = h_\infty(V_s)$, which can be found from the peak value of the current $I_s \approx \bar{g} \cdot 1 \cdot h_s(V_s - E)$. Repeating this experiment for various pre-step potentials, one can determine the steady-state inactivation curve $h_\infty(V)$ in Fig.2.11. In exercise 6 we describe a better method to determine $h_\infty(V)$ that does not rely on the difference between the activation and inactivation time scales.

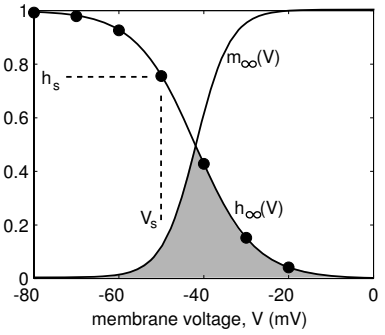

Figure 2.11: Steady-state activation function $m_\infty(V)$ from Fig.2.10, and inactivation function $h_\infty(V)$ and values h_s from Fig.2.12. Their overlap (shaded region) produces a noticeable, persistent "window" current.

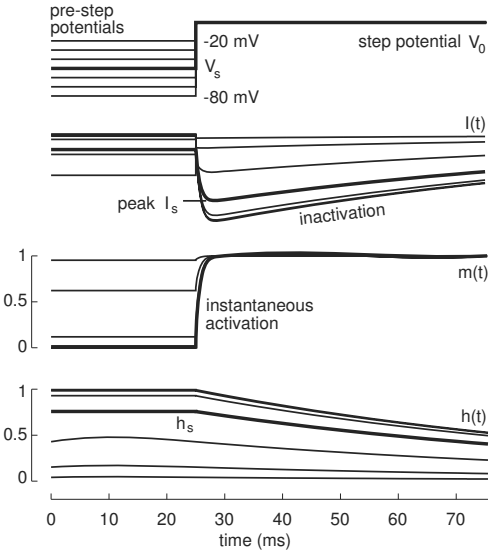

Figure 2.12: Dynamics of the current (I), activation (m), and inactivation (h) variables in the voltage-clamp experiment aimed at measuring $h_\infty(V)$ in Fig.2.11.

The voltage-sensitive steady-state activation and inactivation functions overlap in a shaded window depicted in Fig.2.11. Depending on the size of the shaded area in the figure, the overlap may result in a noticeable "window" current.

2.2.4 Hyperpolarization-Activated Channels

Many neurons in various parts of the brain have channels that are opened by hyperpolarization. These channels produce currents that are turned on by hyperpolarization and turned off by depolarization. Biologists refer to such currents as "exceptional" or "weird", and denote them as $I_{\rm Q}$ (queer), $I_{\rm f}$ (funny), $I_{\rm h}$ (hyperpolarization-activated), or $I_{\rm Kir}$ (K^+ inward rectifier). (We will consider the last two currents in detail in the next chapter). Most neuroscience textbooks classify these currents in a special category – *hyperpolarization-activated currents*. However, from the theoretical point of view, it is inconvenient to create special categories. In this book we treat these currents as

"normal" transient currents with the understanding that they are always activated (either $a = 0$ or variable $m = 1$ in (2.8)), but can be inactivated by depolarization (variable $h \to 0$) or deinactivated by hyperpolarization (variable $h \to 1$). Moreover, there is biophysical evidence suggesting that closing/opening of I_{Kir} is indeed related to the inactivation/deinactivation process (Lopatin et al. 1994).

2.3 The Hodgkin-Huxley Model

In section 2.1 we studied how the membrane potential depends on the membrane currents, assuming that ionic conductances are fixed. In section 2.2 we used the Hodgkin-Huxley gate model to study how the conductances and currents depend on the membrane potential, assuming that the potential is clamped at different values. In this section we put it all together and study how the potential $\leftrightarrow$ current nonlinear interactions lead to many interesting phenomena, such as generation of action potentials.

2.3.1 Hodgkin-Huxley Equations

One of the most important models in computational neuroscience is the Hodgkin-Huxley model of the squid giant axon. Using pioneering experimental techniques of that time, Hodgkin and Huxley (1952) determined that the squid axon carries three major currents: voltage-gated persistent K^+ current with four activation gates (resulting in the term n^4 in the equation below, where n is the activation variable for K^+); voltage-gated transient Na^+ current with three activation gates and one inactivation gate (the term m^3h below), and Ohmic leak current, I_{L}, which is carried mostly by Cl^- ions. The complete set of space-clamped Hodgkin-Huxley equations is

$$\begin{aligned} C\dot{V} &= I - \overbrace{\bar{g}_{\text{K}} n^4 (V - E_{\text{K}})}^{I_{\text{K}}} - \overbrace{\bar{g}_{\text{Na}} m^3 h (V - E_{\text{Na}})}^{I_{\text{Na}}} - \overbrace{g_{\text{L}} (V - E_{\text{L}})}^{I_{\text{L}}} \\ \dot{n} &= \alpha_n(V)(1-n) - \beta_n(V) n \\ \dot{m} &= \alpha_m(V)(1-m) - \beta_m(V) m \\ \dot{h} &= \alpha_h(V)(1-h) - \beta_h(V) h \,, \end{aligned}$$

where

$$\begin{aligned} \alpha_n(V) &= 0.01 \frac{10 - V}{\exp(\frac{10-V}{10}) - 1} \,, \\ \beta_n(V) &= 0.125 \exp\left(\frac{-V}{80}\right) \,, \\ \alpha_m(V) &= 0.1 \frac{25 - V}{\exp(\frac{25-V}{10}) - 1} \,, \\ \beta_m(V) &= 4 \exp\left(\frac{-V}{18}\right) \,, \end{aligned}$$

$$\begin{aligned} \alpha_h(V) &= 0.07 \exp\left(\frac{-V}{20}\right) , \\ \beta_h(V) &= \frac{1}{\exp(\frac{30-V}{10}) + 1} . \end{aligned}$$

These parameters, provided in the original Hodgkin and Huxley paper, correspond to the membrane potential shifted by approximately 65 mV, so that the resting potential is at $V \approx 0$. Hodgkin and Huxley did that for the sake of convenience, but the shift has led to a lot of confusion over the years. The shifted Nernst equilibrium potentials are

$$E_{\rm K} = -12 \text{ mV} , \qquad E_{\rm Na} = 120 \text{ mV} , \qquad E_{\rm L} = 10.6 \text{ mV};$$

(see also exercise 1). Typical values of maximal conductances are

$$\bar{g}_{\rm K} = 36 \text{ mS/cm}^2 , \qquad \bar{g}_{\rm Na} = 120 \text{ mS/cm}^2 , \qquad g_{\rm L} = 0.3 \text{ mS/cm}^2.$$

$C = 1\,\mu\text{F/cm}^2$ is the membrane capacitance and $I = 0\,\mu\text{A/cm}^2$ is the applied current. The functions $\alpha(V)$ and $\beta(V)$ describe the transition rates between open and closed states of the channels. We present this notation only for historical reasons. In the rest of the book, we use the standard form

$$\begin{aligned} \dot{n} &= (n_\infty(V) - n)/\tau_n(V) , \\ \dot{m} &= (m_\infty(V) - m)/\tau_m(V) , \\ \dot{h} &= (h_\infty(V) - h)/\tau_h(V) , \end{aligned}$$

where

$$\begin{aligned} n_\infty &= \alpha_n/(\alpha_n + \beta_n) , & \tau_n &= 1/(\alpha_n + \beta_n) , \\ m_\infty &= \alpha_m/(\alpha_m + \beta_m) , & \tau_m &= 1/(\alpha_m + \beta_m) , \\ h_\infty &= \alpha_h/(\alpha_h + \beta_h) , & \tau_h &= 1/(\alpha_h + \beta_h) \end{aligned}$$

as depicted in Fig.2.13. These functions can be approximated by the Boltzmann and Gaussian functions; see Ex. 4. We also shift the membrane potential back to its true value, so that the resting state is near -65 mV.

The membrane of the squid giant axon carries only two major currents: transient Na^+ and persistent K^+. Most neurons in the central nervous system have additional currents with diverse activation and inactivation dynamics, which we summarize in section 2.3.5. The Hodgkin-Huxley formalism is the most accepted model to describe their kinetics.

Since we are interested in geometrical and qualitative methods of analysis of neuronal models, we assume that all variables and parameters have appropriate scales and dimensions, but we do not explicitly state them. An exception is the membrane potential V, whose mV scale is stated in every figure.

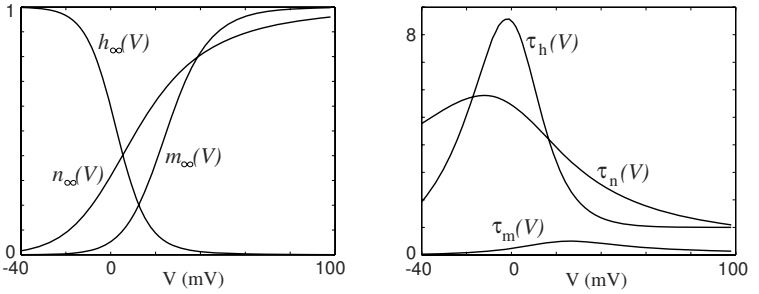

Figure 2.13: Steady-state (in)activation functions (left) and voltage-dependent time constants (right) in the Hodgkin-Huxley model.

Figure 2.14: Studies of spike-generation mechanism in "giant squid" axons won Alan Hodgkin and Andrew Huxley the 1963 Nobel Prize for physiology or medicine (shared with John Eccles). See also Fig. 4.1 in Keener and Sneyd (1998).

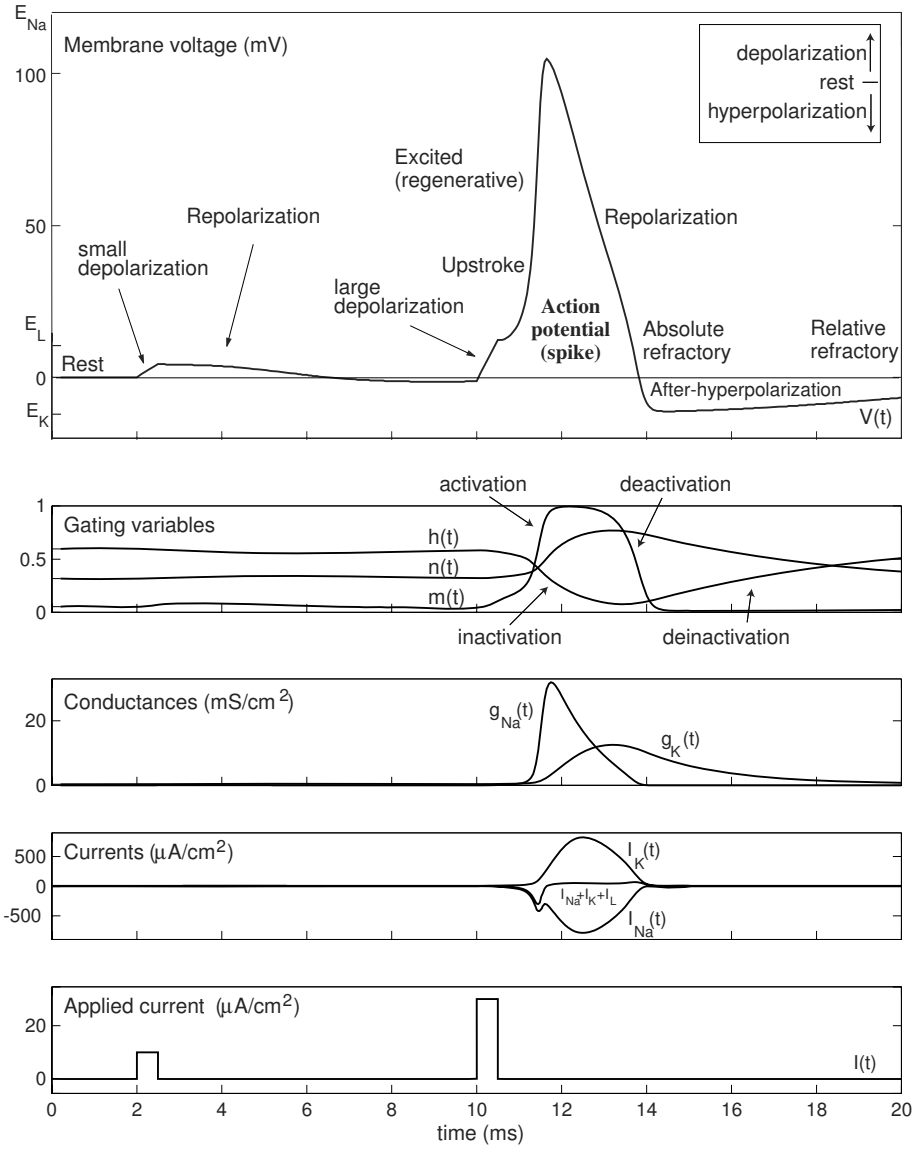

Figure 2.15: Action potential in the Hodgkin-Huxley model.

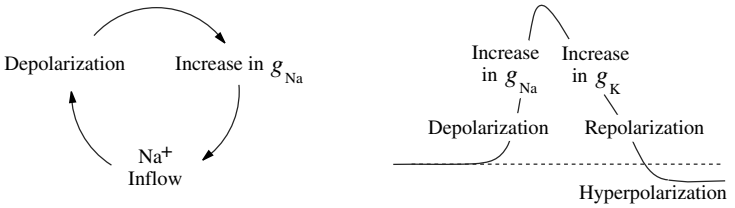

Figure 2.16: Positive and negative feedback loops resulting in excited (regenerative) behavior in neurons.

2.3.2 Action Potential

Recall that when $V = V_{\text{rest}}$, which is 0 mV in the Hodgkin-Huxley model, all inward and outward currents balance each other so the net current is zero, as in Fig.2.15. The resting state is stable: a small pulse of current applied via $I(t)$ produces a small positive perturbation of the membrane potential (depolarization), which results in a small net current that drives V back to resting (repolarization). However, an intermediate size pulse of current produces a perturbation that is amplified significantly because membrane conductances depend on V. Such a nonlinear amplification causes V to deviate considerably from V_{rest} – a phenomenon referred to as an *action potential* or *spike*.

In Fig.2.15 we show a typical time course of an action potential in the Hodgkin-Huxley system. Strong depolarization increases activation variables m and n and decreases inactivation variable h. Since $\tau_m(V)$ is relatively small, variable m is relatively fast. Fast activation of Na^+ conductance drives V toward E_{Na}, resulting in further depolarization and further activation of g_{Na}. This positive feedback loop, depicted in Fig.2.16, results in the *upstroke* of V. While V moves toward E_{Na}, the slower gating variables catch up. Variable $h \to 0$, causing inactivation of the Na^+ current, and variable $n \to 1$, causing slow activation of the outward K^+ current. The latter and the leak current repolarize the membrane potential toward V_{rest}.

When V is near V_{rest}, the voltage-sensitive time constants $\tau_{\text{n}}(V)$ and $\tau_{\text{h}}(V)$ are relatively large, as one can see in Fig.2.13. Therefore, recovery of variables n and h is slow. In particular, the outward K^+ current continues to be activated (n is large) even after the action potential downstroke, thereby causing V to go below V_{rest} toward E_{K} – a phenomenon known as *afterhyperpolarization*.

In addition, the Na^+ current continues to be inactivated (h is small) and not available for any regenerative function. The Hodgkin-Huxley system cannot generate another action potential during this *absolute refractory* period. While the current deinactivates, the system becomes able to generate an action potential, provided the stimulus is relatively strong (*relative refractory* period).

To study the relationship between these refractory periods, we stimulate the Hodgkin-Huxley model with 1-ms pulses of current having various amplitudes and latencies. The

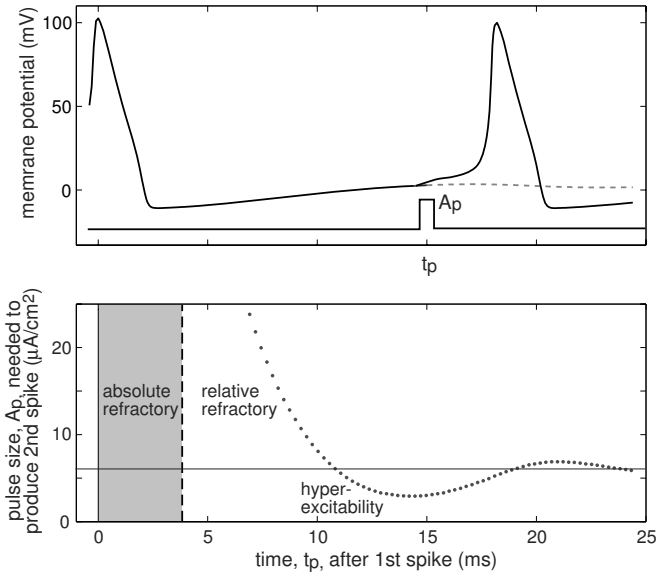

Figure 2.17: Refractory periods in the Hodgkin-Huxley model with $I = 3$.

minimal amplitude of the stimulation needed to evoke a second spike in the model is depicted in Fig.2.17 (bottom). Notice that around 14 ms after the first spike, the model is hyper-excitable, that is, the stimulation amplitude is less than the baseline amplitude $A_p \approx 6$ needed to evoke a spike from the resting state. This occurs because the Hodgkin-Huxley model exhibits damped oscillations of membrane potential (discussed in chapter 7).

2.3.3 Propagation of the Action Potentials

The space-clamped Hodgkin-Huxley model of the squid giant axon describes non-propagating action potentials since $V(t)$ does not depend on the location, x, along the axon. To describe propagation of action potentials (pulses) along the axon having potential $V(x,t)$, radius a (cm), and intracellular resistivity R (Ω·cm), the partial derivative V_{xx} is added to the voltage equation to account for axial currents along the membrane. The resulting nonlinear parabolic partial differential equation

$$C\,V_t = \frac{a}{2R}\,V_{xx} + I - I_{\rm K} - I_{\rm Na} - I_{\rm L}$$

is often referred to as the Hodgkin-Huxley cable or propagating equation. Its important type of solution, a traveling pulse, is depicted in Fig.2.18. Studying this equation goes beyond the scope of this book; the reader can consult Keener and Sneyd (1998) and references therein.

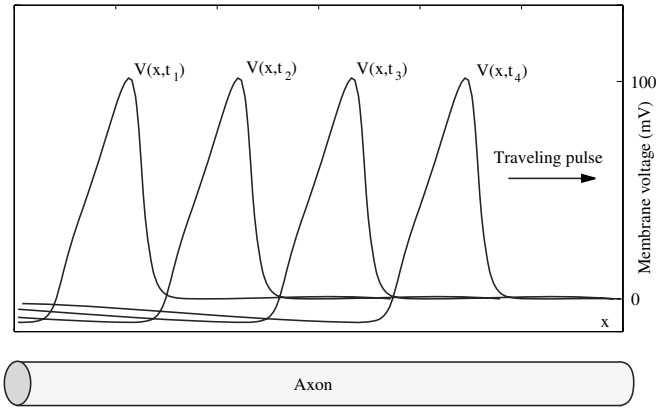

Figure 2.18: Traveling pulse solution of the Hodgkin-Huxley cable equation at four successive moments.

2.3.4 Dendritic Compartments

Modifications of the Hodgkin-Huxley model, often called Hodgkin-Huxley-type models or conductance-based models, can describe the dynamics of spike-generation of many, if not all, neurons recorded in nature. However, there is more to the computational property of neurons than just the spike-generation mechanism. Many neurons have an extensive dendritic tree that can sample the synaptic input arriving at different locations and integrate it over space and time.

Many dendrites have voltage-gated currents, so the synaptic integration is non-linear, sometimes resulting in dendritic spikes that can propagate forward to the soma of the neuron or backward to distant dendritic locations. Dendritic spikes are prominent in intrinsically bursting (IB) and chattering (CH) neocortical neurons considered in chapter 8. In that chapter we also model regular spiking (RS) pyramidal neurons, the most numerous class of neurons in mammalian neocortex, and show that their spike-generation mechanism is one of the simplest. The computation complexity of RS neurons must be hidden, then, in the arbors of their dendritic trees.

It is not feasible at present to study the dynamics of membrane potential in dendritic trees either analytically or geometrically (i.e., without resort to computer simulations), unless dendrites are assumed to be passive (linear) and semi-infinite, and to satisfy Rall's branching law (Rall 1959). Much of the insight can be obtained via simulations, which typically replace the continuous dendritic structure in Fig.2.19a with a network of discrete compartments in Fig.2.19b. Dynamics of each compartment is simulated by a Hodgkin-Huxley-type model, and the compartments are coupled via conductances. For example, if V_s and V_d denote the membrane potential at the soma and in the dendritic tree, respectively, as in Fig.2.19c, then

$$C_s\dot{V}_s = -I_s(V_s,t) + g_s(V_d - V_s)\ , \qquad \text{and} \qquad C_d\dot{V}_d = -I_d(V_d,t) + g_d(V_s - V_d)\ ,$$

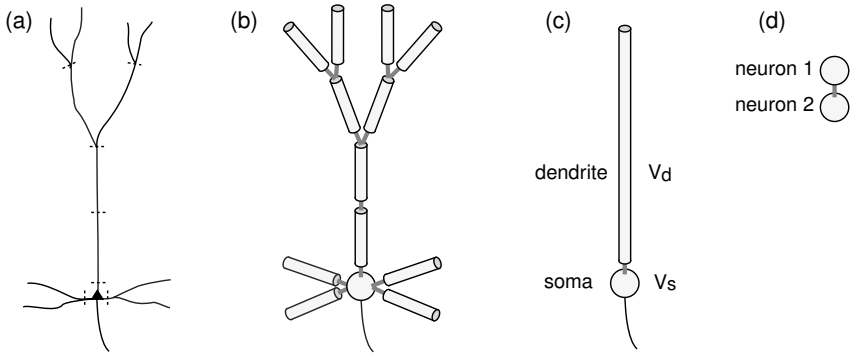

Figure 2.19: A dendritic tree of a neuron (a) is replaced by a network of compartments (b), each modeled by a Hodgkin-Huxley-type model. The two-compartment neuronal model (c) may be equivalent to two neurons coupled via gap junctions (electrical synapse) (d).

where each $I(V,t)$ represents the sum of all voltage-, Ca^{2+}-, and time-dependent currents in the compartment, and g_s and g_d are the coupling conductances that depend on the relative sizes of dendritic and somatic compartments. One can obtain many spiking and bursting patterns by changing the conductances and keeping all the other parameters fixed (Pinsky and Rinzel 1994, Mainen and Sejnowski 1996).

Once we understand how to couple two compartments, we can do it for hundreds or thousands of compartments. GENESIS and NEURON simulation environments could be useful here, especially since they contain databases of dendritic trees reconstructed from real neurons.

Interestingly, the somatic-dendritic pair in Fig.2.19c is equivalent to a pair of neurons in Fig.2.19d coupled via *gap-junctions*. These are electrical contacts that allow ions and small molecules to pass freely between the cells. Gap junctions are often called electrical synapses, because they allow potentials to be conducted directly from one neuron to another.

Computational study of multi-compartment dendritic processing is outside of the scope of this book. We consider multi-compartment models of cortical pyramidal neurons in chapter 8 and gap-junction coupled neurons in chapter 10 (which is on the author's webpage).

2.3.5 Summary of Voltage-Gated Currents

Throughout this book we model kinetics of various voltage-sensitive currents using the Hodgkin-Huxley gate model

$$I = \bar{g}\, m^a h^b (V - E)$$

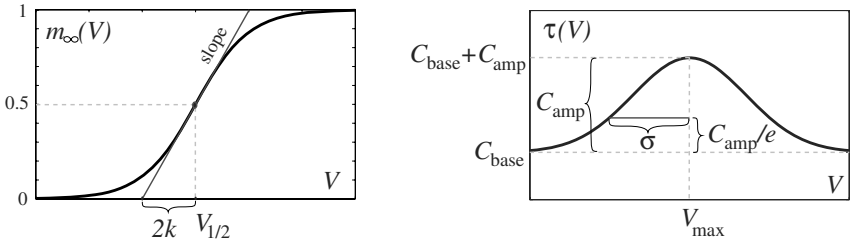

Figure 2.20: Boltzmann (2.11) and Gaussian (2.12) functions and geometrical interpretations of their parameters.

where
I - current , (μA/cm^2),
V - membrane voltage, (mV),
E - reverse potential, (mV),
$\bar{g}$ - maximal conductance, (mS/cm^2),
m - probability of activation gate to be open,
h - probability of inactivation gate to be open,
a - the number of activation gates per channel,
b - the number of inactivation gates per channel.
The gating variables m and n satisfy linear first-order differential equations (2.9) and (2.10), respectively. We approximate the steady-state activation curve $m_\infty(V)$ by the Boltzmann function depicted in Fig.2.20,

$$m_\infty(V) = \frac{1}{1 + \exp\{(V_{1/2} - V)/k\}} \tag{2.11}$$

The parameter $V_{1/2}$ satisfies $m_\infty(V_{1/2}) = 0.5$, and k is the slope factor (negative for the inactivation curve $h_\infty(V)$). Smaller values of $|k|$ result in steeper $m_\infty(V)$.

The voltage-sensitive time constant $\tau(V)$ can be approximated by the Gaussian function

$$\tau(V) = C_{\text{base}} + C_{\text{amp}} \exp \frac{-(V_{\max} - V)^2}{\sigma^2} , \tag{2.12}$$

see Fig.2.20. The graph of the function is above C_{base} with amplitude C_{amp}. The maximal value is achieved at $V_{\max}$. The parameter σ measures the characteristic width of the graph, that is, $\tau(V_{\max} \pm \sigma) = C_{\text{base}} + C_{\text{amp}}/e$. The Gaussian description is often not adequate, so we replace it with other functions whenever appropriate.

Below is the summary of voltage-gated currents whose kinetics were measured experimentally. The division into persistent and transient is somewhat artificial, since most "persistent" currents can still inactivate after seconds of prolonged depolarization. Hyperpolarization-activated currents, such as the h-current or K^+ inwardly rectifying current, are mathematically equivalent to currents that are always activated, but can be inactivated by depolarization. To avoid possible confusion, we mark these currents "opened by hyperpolarization".

Na^+ currents	Parameters (Fig.2.20) Eq. (2.11) $V_{1/2}$	k	Eq. (2.12) V_{max}	σ	C_{amp}	C_{base}
Fast transient [1]	$I_{Na,t} = \bar{g}\, m^3 h(V - E_{Na})$					
activation	−40	15	−38	30	0.46	0.04
inactivation	−62	−7	−67	20	7.4	1.2
Fast transient [2]	$I_{Na,t} = \bar{g}\, m_\infty(V) h(V - E_{Na})$					
activation	−30	5.5	–	–	–	–
inactivation	−70	−5.8	$\tau_h(V) = 3\exp((-40 - V)/33)$			
Fast transient [3]	$I_{Na,t} = \bar{g}\, m_\infty(V) h(V - E_{Na})$					
activation	−28	6.7	–	–	–	–
inactivation	−66	−6	$\tau_h(V) = 4\exp((-30 - V)/29)$			
Fast persistent [4,a]	$I_{Na,p} = \bar{g}\, m_\infty(V) h(V - E_{Na})$					
activation	−50	4	–	–	–	–
inactivation	−49	−10	−66	35	4.5 sec	2 sec
Fast persistent [5,a]	$I_{Na,p} = \bar{g}\, m_\infty(V)(0.14 + 0.86h)(V - E_{Na})$					
activation	−50	6	–	–	–	–
inactivation	−56	−7	$\tau_h(V) = 63.2 + 25\exp(-V/25.5)$			
Fast persistent [2]	$I_{Na,p} = \bar{g}\, m(V - E_{Na})$					
activation	−54	9	–	–	–	0.8
Fast persistent [6]	$I_{Na,p} = \bar{g}\, m(V - E_{Na})$					
activation	−42	4	–	–	–	0.8

1. Squid giant axon (Hodgkin and Huxley 1952); see exercise 4.
2. Thalamocortical neurons in rats (Parri and Crunelli 1999).
3. Thalamocortical neurons in cats (Parri and Crunelli 1999).
4. Layer-II principal neurons in entorhinal cortex (Magistretti and Alonso 1999).
5. Large dorsal root ganglion neurons in rats (Baker and Bostock 1997, 1998).
6. Purkinje cells (Kay et al. 1998).

a Very slow inactivation.

K^+ currents	Parameters (Fig.2.20) Eq. (2.11) $V_{1/2}$	k	Eq. (2.12) V_{max}	σ	C_{amp}	C_{base}
Delayed rectifier [1]	$I_K = \bar{g}\, n^4(V - E_K)$					
activation	−53	15	−79	50	4.7	1.1
Delayed rectifier [2,4]	$I_K = \bar{g}\, mh(V - E_K)$					
activation	−3	10	−50	30	47	5
inactivation	−51	−12	−50	50	1000	360
M current [3]	$I_{K(M)} = \bar{g}\, m(V - E_K)$					
activation	−44	8	−50	25	320	20
Transient [4]	$I_A = \bar{g}\, mh(V - E_K)$					
activation	−3	20	−71	60	0.92	0.34
inactivation	−66	−10	−73	23	50	8
Transient [5]	$I_A = \bar{g}\, mh(V - E_K)$					
activation	−26	20	–	–	–	–
inactivation	−72	−9.6	–	–	–	15.5
Transient [6]	$I_A = \bar{g}\, m^4 h\,(V - E_K)$					
Fast component (60% of total conductance)						
activation	−60	8.5	−58	25	2	0.37
inactivation	−78	−6	−78	25	45	19
Slow component (40% of total conductance)						
activation	−36	20	−58	25	2	0.37
inactivation	−78	−6	−78	25	45	19
			$\tau_h(V) = 60$ when $V > -73$			
Inward rectifier [7] (*opened by hyperpolarization*)	$I_{Kir} = \bar{g}\, h_\infty(V)(V - E_K)$					
inactivation	−80	−12	–	–	–	< 1

1. Squid giant axon (Hodgkin and Huxley 1952); see exercise 4.
2. Neocortical pyramidal neurons (Bekkers 2000).
3. Rodent neuroblastoma-glioma hybrid cells (Robbins et al. 1992).
4. Neocortical pyramidal neurons (Korngreen and Sakmann 2000).
5. Hippocampal mossy fiber boutons (Geiger and Jonas 2000).
6. Thalamic relay neurons (Huguenard and McCormick 1992).
7. Horizontal cells in catfish retina (Dong and Werblin 1995); AP cell of leech (Wessel et al. 1999); rat locus coeruleus neurons (Williams et al. 1988, $V_{1/2} = E_K$).

Cation currents	Parameters (Fig.2.20) Eq. (2.11) $V_{1/2}$	k	Eq. (2.12) $V_{\max}$	σ	C_{amp}	C_{base}
I_{h} current [1] ($\textit{opened by hyperpolarization}$)	$I_{\text{h}} = \bar{g}\, h\, (V - E_{\text{h}})$,		$E_{\text{h}} = -43$ mV			
inactivation	-75	-5.5	-75	15	1000	100
I_{h} current [2]	$I_{\text{h}} = \bar{g}\, h\, (V - E_{\text{h}})$,		$E_{\text{h}} = -1$ mV			
inact. (soma)	-82	-9	-75	20	50	10
inact. (dendrite)	-90	-8.5	-75	20	40	10
I_{h} current [3]	$I_{\text{h}} = \bar{g}\, h\, (V - E_{\text{h}})$,		$E_{\text{h}} = -21$ mV			
fast inact. (65%)	-67	-12	-75	30	50	20
slow inact. (35%)	-58	-9	-65	30	300	100

1. Thalamic relay neurons (McCormick and Pape 1990; Huguenard and McCormick 1992).
2. Hippocampal pyramidal neurons in CA1 (Magee 1998).
3. Entorhinal cortex layer II neurons (Dickson et al. 2000).

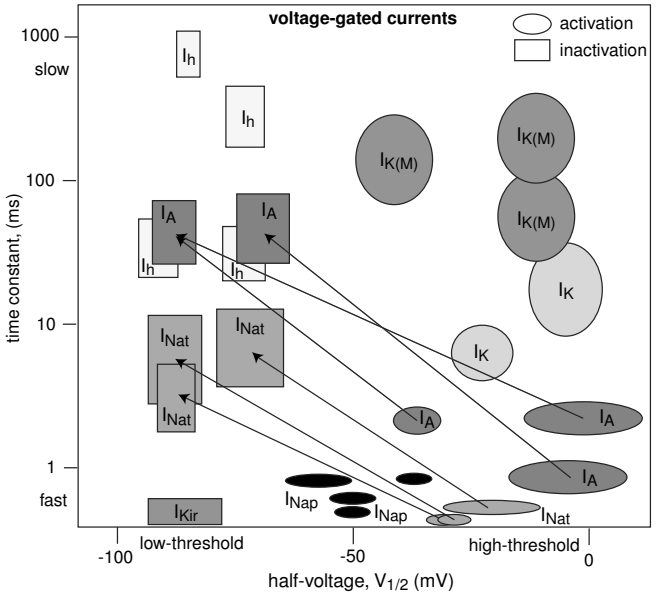

Figure 2.21: Summary of current kinetics. Each oval (rectangle) denotes the voltage and temporal scale of activation (inactivation) of a current. Transient currents are represented by arrows connecting ovals and rectangles.

Figure 2.22: Alan Hodgkin (right) and Andrew Huxley (left) in their Plymouth Marine Lab in 1949. (Photo provided by National Marine Biological Library, Plymouth, UK).

Review of Important Concepts

- Electrical signals in neurons are carried by Na^+, Ca^{2+}, K^+, and Cl^- ions, which move through membrane channels according to their electrochemical gradients.
- The membrane potential V is determined by the membrane conductances g_i and corresponding reversal potentials E_i:

$$C\,\dot{V} = I - \sum_i g_i \cdot (V - E_i)\ .$$

- Neurons are excitable because the conductances depend on the membrane potential and time.
- The most accepted description of kinetics of voltage-sensitive conductances is the Hodgkin-Huxley gate model.
- Voltage-gated activation of inward Na^+ or Ca^{2+} current depolarizes (increases) the membrane potential.
- Voltage-gated activation of outward K^+ or Cl^- current hyperpolarizes (decreases) the membrane potential.
- An action potential or spike is a brief regenerative depolarization of the membrane potential followed by its repolarization and possibly hyperpolarization, as in Fig.2.16.

Bibliographical Notes

Our summary of membrane electrophysiology is limited: we present only those concepts that are necessary to understand the Hodgkin-Huxley description of generation of action potentials. We have omitted such important topics as the Goldman-Hodgkin-Katz equation, cable theory, dendritic and synaptic function, although some of those will be introduced later in the book.

The standard textbook on membrane electrophysiology is the second edition of *Ion Channels of Excitable Membranes* by B. Hille (2001). An excellent introductory textbook with an emphasis on the quantitative approach is *Foundations of Cellular Neurophysiology* by D. Johnston and S. Wu (1995). A detailed introduction to mathematical aspects of cellular biophysics can be found in *Mathematical Physiology* by J. Keener and J. Sneyd (1998). The latter two books complement rather than repeat each other. *Biophysics of Computation* by Koch (1999) and chapters 5 and 6 of *Theoretical Neuroscience* by Dayan and Abbott (2001) provide a good introduction to biophysics of excitable membranes.

The first book devoted exclusively to dendrites is *Dendrites* by Stuart et al. (1999). It emphasizes the active nature of dendritic dynamics. Arshavsky et al. (1971; Russian language edition, 1969) make the first, and probably still the best, theoretical attempt to understand the neurocomputational properties of branching dendritic trees endowed with voltage-gated channels and capable of generating action potentials. Had they published their results in the 1990s, they would have been considered classics in the field. Unfortunately, the computational neuroscience community of the 1970s was not ready to accept the "heretic" idea that dendrites can fire spikes, that spikes can propagate backward and forward along the dendritic tree, that EPSPs can be scaled-up with distance, that individual dendritic branches can perform coincidence detection and branching points can perform nonlinear summation, and that different and independent computations can be carried out at different parts of the neuronal dendritic tree. We touch on some of these issues in chapter 8.

Exercises

1. Determine the Nernst equilibrium potentials for the membrane of the squid giant axon using the following data:

	Inside (mM)	Outside (mM)
K^+	430	20
Na^+	50	440
Cl^-	65	560

   and $T = 20°C$.

2. Show that a nonselective cation current

$$I = \bar{g}_{Na}\, p\, (V - E_{Na}) + \bar{g}_{K}\, p\, (V - E_{K})$$

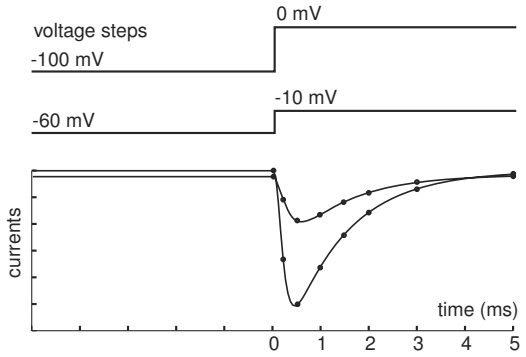

Figure 2.23: Current traces corresponding to voltage steps of various amplitudes; see exercise 6.

can be written in the form (2.7) with

$$\bar{g} = \bar{g}_{\rm Na} + \bar{g}_{\rm K} \qquad \text{and} \qquad E = \frac{\bar{g}_{\rm Na}E_{\rm Na} + \bar{g}_{\rm K}E_{\rm K}}{\bar{g}_{\rm Na} + \bar{g}_{\rm K}} \ .$$

3. Show that applying a DC current I in the neuronal model

$$C\dot{V} = I - g_{\rm L}(V - E_{\rm L}) - I_{\rm other}(V)$$

is equivalent to changing the leak reverse potential $E_{\rm L}$.

4. Steady-state (in)activation curves and voltage-sensitive time constants can be approximated by the Boltzmann (2.11) and Gaussian (2.12) functions, respectively, depicted in Fig.2.20. Explain the meaning of the parameters $V_{1/2}, k$, $C_{\rm base}, C_{\rm amp}, V_{\rm max}$, and σ and find their values that provide satisfactory fit near the rest state $V = 0$ for the Hodgkin-Huxley functions depicted in Fig.2.13.

5. (Willms et al. 1999) Consider the curve $m_\infty^p(V)$, where $m_\infty(V)$ is the Boltzmann function with parameters $V_{1/2}$ and k, and $p > 1$. This curve can be approximated by another Boltzmann function with some parameters $\tilde{V}_{1/2}$ and $\tilde{k}$ (and $p = 1$). Find the formulas that relate $\tilde{V}_{1/2}$ and $\tilde{k}$ to $V_{1/2}$, k, and p.

6. (Willms et al. 1999) Write a MATLAB program that determines activation and inactivation parameters via a simultaneous fitting of current traces from a voltage-clamp experiment similar to the one in Fig.2.23. Assume that the values of the voltage pairs – e.g., $-60, -10; -100, 0$ (mV) – are in the file `v.dat`. The values of the current (circles in Fig.2.23) are in the file `current.dat`, and the sampling times – e.g., 0, 0.25, 0.5, 1, 1.5, 2, 3, 5 (ms) – are in the file `times.dat`.

7. Modify the MATLAB program from exercise 6 to handle multi-step (Fig.2.24) and ramp protocols.

8. **[M.S.]** Find the best sequence of step potentials that can determine activation and inactivation parameters (a) in the shortest time, (b) with the highest precision.

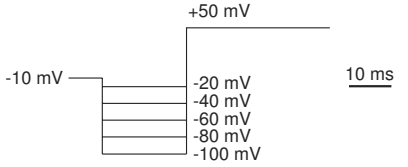

Figure 2.24: Multiple voltage steps are often needed to determine time constants of inactivation; see exercise 7.

9. **[M.S.]** Modify the MATLAB program from exercise 6 to handle multiple currents.

10. **[M.S.]** Add a PDE solver to the MATLAB program from exercise 6 to simulate poor space and voltage clamp conditions.

11. **[Ph.D.]** Introduce numerical optimization into the dynamic clamp protocol to analyze experimentally in real time the (in)activation parameters of membrane currents.

12. **[Ph.D.]** Use new classification of families of channels (Kv3,1, $Na_v1.2$, etc.; see Hille 2001) to determine the kinetics of each subgroup, and provide a complete table similar to those in section 2.3.5.